NASA TECHNICAL MEMORANDUM

NASA TM 73696

NASA TM 73696

PERFORMANCE AT MACH 3.52 OF A MACH 2.5 ALL EXTERNAL-COMPRESSION, TWO-DIMENSIONAL INLET

by Robert W. Cubbison
Lewis Research Center
Cleveland, Ohio 44135

June 1977

1 Report No. NASA TM 73696	2. Government Accession No.	3. Recipient's Catalog No
4. Title and Subtitle PERFORMANCE AT MACH 3.52 OF A MACH 2.5 ALL EXTERNAL-COMPRESSION, TWO-DIMENSIONAL INLET		5. Report Date 6. Performing Organization Code
7. Author(s) Robert W. Cubbison		8. Performing Organization Report No E-9235
9. Performing Organization Name and Address National Aeronautics and Space Administration Lewis Research Center Cleveland, Ohio 44135		10 Work Unit No 11. Contract or Grant No
12. Sponsoring Agency Name and Address National Aeronautics and Space Administration Washington, D. C. 20546		13 Type of Report and Period Covered Technical Memorandum 14. Sponsoring Agency Code
15. Supplementary Notes		

16 Abstract

A quick-look test was conducted in the 10- by 10-foot supersonic wind tunnel to provide some qualitative information on operating a low Mach number design inlet in a highly oversped condition. The model which is a two-dimensional, three-ramp, all-external-compression inlet designed to match a J-85 turbojet engine at Mach 2.5 was run at Mach 3.52 and zero angle-of-attack and yaw. Results are presented snowing the effect of external ramp angle combinations, diffuser ramp position and the amount of bleed.

17. Key Words (Suggested by Author(s)) Inlets Intakes	18. Distribution Statement Unclassified - unlimited STAR Category 02		
19. Security Classif (of this report) Unclassified	20 Security Classif. (of this page) Unclassified	21. No. of Pages	22. Price*

* For sale by the National Technical Information Service Springfield Virginia 22161

PERFORMANCE AT MACH 3.52 OF A MACH 2.5 ALL EXTERNAL-COMPRESSION, TWO-DIMENSIONAL INLET

by Robert W. Cubbison

National Aeronautics and Space Administration
Lewis Research Center
Cleveland, Ohio 44135

E-9235

SUMMARY

A quick-look test was conducted in the Lewis 10- by 10-foot supersonic wind tunnel to provide some qualitative information on operating a low Mach number design inlet in a highly oversped condition. The model which is a two-dimensional, three-ramp, all-external-compression inlet designed to match a J-85 turbojet engine at Mach 2.5 was run at Mach 3.52 and zero angle-of-attack and yaw. The inlet was operated as both a fixed and variable geometry inlet.

For the fixed geometry inlet the second and third ramp angles were kept at the Mach 2.5 position of 10 and 11 degrees, respectively. Severe buzz occurred at Mach 3.52 and attempts to eliminate it by increasing the angle of attack to increase the fixed first ramp angle were unsuccessful.

In the variable geometry phase, three sets of angle combinations were used; $18^\circ + 5^\circ$, $15^\circ + 13^\circ$, and $15.37^\circ + 9.58^\circ$. The latter set were experimentally found to be those for shock-on-lip operation. The theoretically predicted capture mass-flow ratio for the $15.37^\circ + 9.58^\circ$ combination was 0.99 for zero cutback in the side fairings. Experimentally the capture mass-flow ratio was 0.05 less than predicted due to spillage over the cutback side fairings and cowl.

The results of optimizing the diffuser ramp position (bleed door 90 percent open) were the $18^\circ + 5^\circ$ combination produced the highest recovery (0.433) and the lowest distortion (0.055). The $15^\circ + 13^\circ$ combination bled the least amount of flow (0.111) while the $15.37^\circ + 9.58^\circ$ combination captured the most flow (0.927) and delivered the most to the engine (0.79). The dynamic distortion level was 0.04 to 0.06 of the average compressor face total pressure in all cases. Using the optimum fourth ramp setting and reducing the amount of ramp bleed indicated the $18^\circ + 5^\circ$ combination again produced the highest recovery (0.441) and lowest distortion (0.125). Again the $15.37^\circ + 9.58^\circ$ combination captured the most flow (0.892) and delivered the most to the engine (0.812). This combination also bled the least (0.079). Reducing the bleed did not affect the dynamic distortion levels in any of the three ramp angle configurations.

INTRODUCTION

Generally, the approach taken in the design of inlets is to provide high-recovery, shock-on-lip operation at the cruise Mach number. Another approach could be to design the inlet for shock-on-lip operation at a lower Mach number and overspeed it to the high cruise condition. An inlet so designed would be smaller and have zero spillage drag over the entire overspeed range. However, a rapid reduction in the internal performance is inherent in overspeeding a low Mach number design inlet. In contrast, an inlet designed for the high Mach cruise condition maintains relatively high performance over the entire Mach range. However, this higher performance must be tempered by the larger drag due to both the larger inlet plus the spillage drag incurred. A measure of the internal performance of the inlets is necessary to make meaningful comparisons between the two approaches. Considerable information is contained in the literature on the off-design performance of high Mach number design inlets. However, little information is available on low Mach number inlets run in a highly oversped condition. To provide some qualitative information in this area, a quick-look test was added to a current Mach 2.5 inlet dynamic distortion program using a two-dimensional, external-compression inlet. For this overspeed test, the inlet was operated at M = 3.52 (the maximum Mach number in the 10- by 10-foot supersonic wind tunnel). The results of this testing are the subject of this report.

LIST OF SYMBOLS

BL	ramp bleed door position in percent of full open
D	compressor face annulus height, 14.75 cm
d	radial distance from hub of compressor face
dist	steady-state total pressure distortion, $P_{2,\ell_{max}} - P_{2,\ell_{min}}/P_2$
H_c	inlet capture height, 40.8 cm at $\alpha = 0^\circ$
M_0	free-stream Mach number
m_{capt}/m_0	capture mass-flow ratio, $m_3 + m_{RB} + m_{SB}/m_0$
m_{RB}/m_0	ramp-bleed mass-flow ratio
m_{SB}/m_0	total side wall bleed mass-flow ratio
m_2/m_0	engine face mass-flow ratio
P_0	free-stream total pressure
P_2	average compressor face total pressure

$P_{2,\ell}$	compressor face local total pressure
P_2/P_0	average compressor face total pressure recovery
P_x	local static pressure
R_e	Reynolds number/meter
RMS	average dynamic total pressure distortion, avg. $\Delta P_{RMS}/P_2$
$w\sqrt{\theta}/\delta$	engine corrected airflow, kgm/sec
x/H_c	axial distance from cowl lip in capture heights
α	angle of attack, deg
β	angle of yaw, deg
ΔP_{RMS}	root-mean-square value of the fluctuating component of the compressor face local total pressure
λ	ramp angle: degrees for 1, 2, 3; centimeters for 4

APPARATUS AND PROCEDURE

A photograph of the model in the tunnel plus schematic views of the inlet are shown in figure 1. It is an all-external-compression type sized to match the J-85 engine at Mach 2.5 in the Lewis 10- by 10-foot supersonic wind tunnel. The two-dimensional compression system (fig. 1(c)) consists of three ramps, the first of which is fixed at a three-degree angle relative to the engine centerline, while the second and third ramps are remotely variable. The subsonic diffuser consists of a remotely variable fourth ramp (about one engine face diameter long) followed by a nearly constant area section of about two engine-face diameters. Both the 10° internal-angle cowl and cutback side fairings have sharp leading edges. The side fairings are swept back to an angle of 20.5° relative to the inlet horizontal centerline. This angle is 5.32° less than the Mach 2.5 shock wave angle for a 9° effective first ramp angle. (Normal inlet operation is at 6° angle-of-attack). A slot located between ramps three and four is the primary system of boundary layer control. This bleed exits overboard through the top surface (fig. 1(b)). A small secondary bleed along the cowl shock line was installed in the side walls. This flow exits overboard through a rearward facing scoop on each side of the inlet (fig. 1(a)). The inlet was mounted above the tunnel centerline and upside down in order to minimize blockage and realize a larger available angle of attack range. The photograph (fig. 1(a)) shows the inlet rolled 30°. For the Mach 3.5 test it was rolled back to 0°.

The inlet-engine compatibility study for which the inlet was built encompassed only the Mach 2.0 to 2.5 portion of the 10- by 10-foot supersonic wind tunnel operating range. At these Mach numbers the free-stream temperature is about 311 K. At Mach 3.5 the temperature is about 422 K. Consequently, when this quick-look test was added at the end of the compatibility study is was necessary to make several modifications to the model. Cooling was added to the position indicators, jumpers on pressure tubes were changed and the elaborate compressor face dynamic instrumentation was replaced with five three-tube rakes. The compressor face tube arrangement is shown in figure 2. Due to the amount of disassembly required to change all jumpers on instrumentation only that which was readily accessible and absolutely needed was changed.

RESULTS AND DISCUSSION

Normally, as the design speed of an inlet is increased the amount or complexity of the variable geometry required is also increased. By operating the inlet in a highly oversped condition it may be possible to completely eliminate the need for variable geometry capability beyond the low-speed, design-point requirements. To explore this concept, the inlet was operated as both a fixed and variable geometry inlet. For the fixed geometry data, the second and third ramp angles (fig. 1(c)) were fixed at the Mach 2.5 positions of 10° and 11°, respectively.

Fixed Geometry

It is obvious from the effect of Mach number on oblique shock angles, that the inlet capture mass-flow of a fixed-geometry inlet quickly increases to 100 percent as the Mach number is increased above design. This satisfies the zero spillage drag during overspeed operation. However, another equally important consideration is the effect of the oblique shocks falling farther inside as the overspeed Mach number is increased. With the inlet operating at critical (terminal shock at the lip), part of the capture flow is subjected to a single shock on the cowl side and part to a multi-shock system on the ramp side separated by one or more vortex sheets trailing aft from the shock intersections. Because of the disparity in losses between the two compression systems, either large distortions (if the flow is stable) or inlet buzz can result. Buzz occurs when the flow in the low energy region is stagnated by the subsonic diffuser increasing the static pressure up to the remaining total pressure. Supercritical operation will delay the onset of this buzz, however, distortion levels will, in general, rise quickly. The fixed geometry configuration was tried at zero degrees angle-of-attack (ramp angles of 3°, 10°, and 11°) with the mass-flow control plug set to position the terminal shock in the ramp bleed slot. Severe buzz occurred. Attempts to alleviate this buzz by increasing angle-of-attack to steepen the shock angles was unsuccessful. Supercritical operation was

not tried. Consequently, no data were recorded for the fixed geometry concept.

Variable Geometry

The basic premise of the variable geometry mode was to subject the entire flow field to more than just normal shock compression. This would reduce the total pressure losses thereby reducing the possibility of buzz due to flow stagnation. Three combinations of the second plus third ramp angles (15.37° + 9.58°, 18° + 5°, and 15° + 13°) were evaluated at zero degrees angle-of-attack. This first set was determined experimentally as the only combination that produced "shock-on-lip" operation. For the other two combinations, the oblique shock system fell ahead of the lip. Theoretical shock patterns determined from a one-dimensional, inviscid analysis are shown in figure 3. The analysis predicted a detached wave at the cowl lip in two cases (figs. 3(a) and (c)) which was confirmed visually in the testing. For the shock-on-lip combination (fig. 3(a)) an increase of 2.2° in the internal cowl angle would prevent detachment and thus the associated spillage. However, the trade-off in drag would have to be evaluated to determine if the 2.2° increase is wanted. The cutback side fairings will spill flow whenever the oblique shocks generated by the ramps appear above the side fairing leading edge. These cutbacks increased the stable range and improved maneuvering capability at the design Mach number. If such capability is not required in an application using an oversped inlet then the cutback can be eliminated thus eliminating the spillage. The analysis indicated a supersonic total pressure recovery of about 0.50 for all three angle combinations and capture mass flow ratios (not adjusted for side wall spillage) of 0.99, 0.95, and 0.90 for the 15.37° + 9 58°, 18° + 5°, and 15° + 13°, respectively.

The effect of fourth ramp position on critical inlet performance is shown in figures 4 through 8. Prior experience at Mach number 2.5 had shown that the performance would maximize at some fourth ramp position below the flush position as defined in figure 1(c). At the lower Mach number it was observed that with the fourth ramp flush and the mass flow control plug set for the assumed critical airflow, the terminal shock was ahead of the cowl lip. As the fourth ramp was lowered (with the mass-flow-control plug fixed), the terminal shock was observed to first move downstream into the inlet, obviously reverse the movement at same fourth ramp position and move forward with further ramp reduction until either buzz occurred or the ramp was fully collapsed. Inlet pressure recovery increased to a maximum and then fell off gradually as the fourth ramp was lowered. This maximum generally occurred at an intermediate fourth ramp position between the shock reversal position and the buzz limit or full collapse. At this height the bleed slot was approximately parallel to the local cowl surface and the fourth ramp angle was generally at or below that where the flow would remain attached to the ramp. Repeating this procedure at

Mach 3.52 it was observed that the inlet responded much in the same manner as it did at Mach 2.5. Critical operation was determined with the fourth ramp flush by positioning the terminal shock at the cowl lip with the mass-flow control plug. As shown in figure 4(a), the performance of the $15.37^{\circ} + 9.58^{\circ}$ ramp angles was still increasing at a fourth ramp position of -2.95 centimeters. At this position some unsteadiness was observed in the visible shock structure and further reduction in height was not tried. Increasing the internal cowl lip angle about 3° to attach the internal shock may alleviate this unsteadiness and permit more fourth ramp movement to optimize the performance. The performance of the $18^{\circ} + 5^{\circ}$ combination (fig. 4(b)) indicates that possibly the optimum could occur at a higher position than the -1.58 centimeter position. The $15^{\circ} + 13^{\circ}$ combination (fig. 4(c)) behaved in the expected manner except for the very high distortion levels encountered. In all three cases the lowest ramp setting shown was the buzz limit position. Based on this limited amount of data on these three ramp angle combinations, the $18^{\circ} + 5^{\circ}$ combination produced the highest recovery (0.433) and lowest distortion (0.055). The $15^{\circ} + 13^{\circ}$ angles bled the least amount of flow (0.111 total) and the $15.37^{\circ} + 9.58^{\circ}$ combination captured the maximum flow (0.927) and delivered the most to the engine (0.79). All three combinations produced RMS levels of about 0.04 to 0.06. The maximum capture for all three combinations was about 0.05 below the predicted values indicating about 0.05 in spillage over the cutback side fairings and cowl. As the fourth ramp was lowered, the capture quantity generally decreased. The reason for this will be discussed later.

Earlier experience at low Mach numbers has shown that distortion levels on the order of 0.15 were indicative of fourth ramp flow separation. The compressor face profiles of figures 5(a) and (b) bear this out. Rakes 1 and 5 (downstream of the fourth ramp) show the flow is separated, however, the trend toward attachment is evident with the $15.37^{\circ} + 9.58^{\circ}$ angles (fig. 5(a)). A fourth ramp position lower than -2.95 centimeters could possibly achieve attachment if the buzz limit can be extended. In figure 5(b)($18^{\circ} + 5^{\circ}$), the -2.59 centimeter position which produced 0.125 distortion shows a tendency for the flow to separate from the fourth ramp. The separation apparent in figure 5(c) ($15^{\circ} + 13^{\circ}$) is on the cowl side. The fourth ramp position is considerably lower to optimize the performance of the $15^{\circ} + 13^{\circ}$ combination than for the other two combinations This ramp position in conjunction with the ramp bleed slot could cause sufficient turning of the flow on the ramp side to pull the flow off of the cowl. The dynamic activity (fig. 6), as expected, is predominately larger in the high flow regions of the diffuser. Although the average dynamic distortion is about 0.04 to 0.06, levels in excess of 10 percent of the average compressor face total pressure level are apparent for all ramp configurations.

Static pressure distributions along the forward position of the inlet cowl are shown in figure 7. The p_x/P_0 for Mach 1.0 shown on

the figure is simply 0.5283 of the cowl lip total pressure recovery estimated from the shock patterns of figure 3. As previously discussed, the inviscid analysis (fig. 3) and schlieren observations show the cowl lip shock wave was attached in one case and detached in the other two cases with an obvious normal shock ahead of the lip in the $15^{\circ} + 13^{\circ}$ case. The data (fig. 7) verify this, in that, the flow entering the cowl lip of the $18^{\circ} + 5^{\circ}$ case is supersonic and subsonic for the $15^{\circ} + 13^{\circ}$ combination. However, in the $15.37^{\circ} + 9.58^{\circ}$ case where the flow angle was 2.2° beyond wave detachment, evidently the flow quickly re-accelerates to supersonic conditions as indicated by the corresponding pressure distributions (fig. 7(a)). The pressure distributions for the $15.37^{\circ} + 9.58^{\circ}$ and the $15^{\circ} + 13^{\circ}$ combinations (figs. 7(a) and (c)) indicate the passage between the cowl lip and fourth ramp leading edge contracts back to the start of the bleed slot and expands across the slot. The expanding region is caused by the flow removal through the bleed. This is evident from the initial compression indicated by the pressure distributions followed by the sharp expansion in this region in the $15.37^{\circ} + 9.58^{\circ}$ case and the initial acceleration of the entering subsonic flow of the $15^{\circ} + 13^{\circ}$ case followed by the change in rate of acceleration at the leading edge of the bleed slot ($\lambda_4 = -5.08$ cm, fig. 7(c)). In the $15.37^{\circ} + 9.58^{\circ}$ case the flow is re-accelerated to supersonic conditions and then passes through the terminal shock which occurs near the rear edge of the bleed. For the $\lambda_4 = -5.08$ centimeter point in the $15^{\circ} + 13^{\circ}$ case, the flow is probably re-accelerated to supersonic conditions followed by a second terminal shock. In the other instances the back pressure prevents choking. Pressure distributions for the $18^{\circ} + 5^{\circ}$ combination (fig. 7(b)) indicate the area is slightly increasing in the first part followed by an additional increase caused by the bleed region. Consequently, the terminal shock will stand anywhere in the region as dictated by the exit corrected airflow. Also, evident for all three configurations is an increase in pressure level in the forward region of the duct as the fourth ramp height is lowered indicating an increased back-pressure level in the inlet. A cross plot of the pressure nearest the cowl lip versus fourth ramp height is shown in figure 8. The $18^{\circ} + 5^{\circ}$ combination shows the small rise as the fourth ramp is lowered and the $15^{\circ} + 13^{\circ}$ combination shows the largest rise as the fourth ramp is lowered. The increases in back-pressure correlate quite well with the decreases in the corresponding capture mass-flows shown in figure 4.

With the fourth ramp set at the selected optimum height, the effect of the amount of ramp bleed on critical inlet performance was determined. The results presented in percent of full door opening are shown in figures 9 through 13. Previous experience at Mach 2.5 has shown that the inlet performance responds to ramp-bleed reduction in a manner similar to that with variations in fourth ramp positions. Decreasing the bleed door exit area caused an increase in pressure recovery with a corresponding increase in engine mass flow for the fixed corrected airflow. The ramp bleed decreased and the side-wall-bleed increased. The distortion and RMS generally increased. Again the

$18^{\circ} + 5^{\circ}$ combination produced the highest recovery (0.441) and the lowest distortion (0.125). The $15.37^{\circ} + 9.58^{\circ}$ combination bled the least (0.079 total) captured the maximum amount of flow (0.892) and delivered the most to the engine (0.812). Again the RMS levels were about 0.04 to 0.06. For a constant corrected airflow an increase in recovery requires an increase in mass-flow. The recovery increases noted here were not large enough to require an engine mass-flow increase equal to the bleed reduction. Consequently, the spillage increased as indicated by the decrease in capture mass-flow. During the testing, small changes were observed to take place in the external shock structure as the bleed opening was reduced. These changes apparently account for the increase in spillage.

Comparing figures 5 and 10, it is apparent that reducing the ramp bleed produced no significant change in the compressor face total pressure profiles. Also, a comparison between figures 6 and 11 (at comparable fourth ramp settings) shows that little change was made in the dynamic pressure profiles when the ramp bleed was reduced. The static pressure distributions (fig. 12) respond in much the same manner with bleed reduction as with fourth ramp variation. The flow in the $15.37^{\circ} + 9.58^{\circ}$ case is again re-accelerated to supersonic conditions by the action of the bleed slot. In the $15^{\circ} + 13^{\circ}$ case, the flow is subsonic for all bleed door settings. The shock positions in the $18^{\circ} + 5^{\circ}$ case are close to the cowl lip for the various door settings. The acceleration produced by the bleed slot is evident in the subsonic flow ($x/H_c \approx 2/7$).

A cross plot of the most forward static pressure is presented in figure 13. These pressures show very little variation compared to those of figure 7. Apparently, the changes visually observed in the external shock structure provided the required spillage without affecting enough of the cowl-side flow field to cause significant changes in pressure levels at the cowl lip station. The pressure change noted in the $15^{\circ} + 13^{\circ}$ case would account for about 25 percent of the change in capture shown in figure 9(c).

Inlet operating maps were obtained for two configurations; the $15.37^{\circ} + 9.58^{\circ}$, -2.74 centimeters, 41 percent door opening and the $18^{\circ} + 5^{\circ}$, -3.1 centimeters, 50 percent door opening. The first configuration was selected because of high capture flow with reasonable recovery while the second was chosen on the basis of recovery and better distortion characteristics. Inlet performance plus the compressor face profiles and static pressure distributions are shown in figure 14 through 17. As previously discussed, optimizing the fourth ramp and bleed door positions resulted in additional spillage from changes in the external shock structure caused by the increase in inlet backpressure. Consequently, in the two cases here, the engine mass flow would be expected to increase as the pressure recovery is reduced. As seen in figure 14, the increase in mass flow (0.75 to 0.775) is more obvious for the $18^{\circ} + 5^{\circ}$ case than for the $15.37^{\circ} + 9.58^{\circ}$ case which was from 0.812 to 0.818. Since the bleed flows (except for the most supercritical point in the $18^{\circ} + 5^{\circ}$ case) remain essentially constant,

the increase in engine mass-flow (0.02) is due to an increase in capture flow. The remaining 0.006 in engine flow is due to the reduction in bleed (primarily the ramp bleed). Only a small increase (0.006) is realized in the 15.37° + 9.58° case. The fairings of the inlet canes were determined from the static pressure distributions shown in figure 15. All points except the minimum stable or peak point show supersonic flow at the aft edge of the bleed slot for the 15.37° + 9.58° configuration (fig. 15(a)). In the 18° + 5° case the last two points show supersonic conditions (fig. 15(b)). Changes in the external flow field can occur until the flow chokes. Therefore, the increases in engine mass-flow were primarily due to changes in the external shock structure until the flow choked and after choking from any bleed reductions that occur. Supercritical operation with the 18° + 5° configuration produced reasonable steady-state distortion levels of 0.06 to 0.125 and dynamic distortion levels of 0.036 to 0.086. The steady-state distortion levels in the 15.37° + 9.58° case increased rapidly from 0.21 to 0.72. The dynamic distortion levels of 0.06 to 0.087 were comparable to those for the 18° + 5° case. The high steady-state levels are due to the flow separating from the fourth ramp. This separation could possibly be alleviated by lowering the fourth ramp further, however, to do this the shock system unsteadiness previously discussed would have to be eliminated. If (as suggested earlier) increasing the cowl lip angle is either not feasible or desirable, then re-contouring the ramp and/or moving the hinge line aft is a possibility. This would reduce the initial angle of the subsonic diffuser by lengthening the fourth ramp which could eliminate the flow separation. An improvement in the Mach 3.52 performance would be expected and could also be beneficial at the lower Mach numbers. The extent of the flow separation is shown in the total pressure profiles of figure 16. Rakes 1 and 4 (fig. 16(a)) show that no flow passes through the ramp side region of the compressor face. At the more supercritical conditions there is some indication of reverse flow in this region. In the flow core (middle of rake 2) the maximum Mach number is near sonic for the most supercritical condition. Total pressure profiles for the 18° + 5° case are shown in figure 16(b). The tip or ramp side portions of rakes 1 and 5 show that separation was eminent if the inlet had been operated more supercritical. The distortion for the last recorded point was 0.125 which is approaching the 0.15 level that experience with this inlet has shown to be associated with separation. The dynamic total pressure profiles are shown in figure 17. As expected, the most turbulence is in the high flow region of the duct and obviously more pronounced in the 15.37° + 9.58° case (fig. 17(b)). Both configurations exhibited about the same average levels (fig. 14). However, the 15.37° + 9.58° configuration displays wide variations across rakes 2 and 3 while the 18° + 5° case shows a much more uniform distribution across the same rakes.

CONCLUSIONS

A quick-look test was conducted in the 10- by 10-foot supersonic wind tunnel to provide some qualitative information on operating a low

Mach number design inlet in a highly oversped condition. The model which is a two-dimensional, three-ramp, all-external-compression inlet designed to match a J-85 turbojet engine at Mach 2.5 was run at Mach 3.52 and zero angle-of-attack and yaw. The inlet was operated as both a fixed and variable geometry inlet. For the fixed geometry portion the second and third ramp angles were fixed at the Mach 2.5 position of ten and eleven degrees, respectively. In the variable geometry phase, three sets of angle combinations ($18^\circ + 5^\circ$, $15^\circ + 13^\circ$, and $15.37^\circ + 9.58^\circ$) were used. The following conclusions were obtained.

1. Using the Mach 2.5 ramp angles (fixed geometry approach) at Mach 3.52 resulted in severe buzz and attempts to eliminate it by increasing the angle-of-attack were unsuccessful.

2. The second and third ramp angles for shock-on-lip operation were experimentally found to be 15.37° and 9.58°, respectively.

3. Theoretical estimates predicted capture mass-flow ratios of 0.99, 0.95, and 0.90 for the $15.37^\circ + 9.58^\circ$, $18^\circ + 5^\circ$, and $15^\circ + 13^\circ$ ramp angle combinations, respectively.

4. The experimentally determined maximum capture mass-flow ratio was 0.05 less than predicted values due to spillage over the outback side fairings and cowl.

5. The results of optimizing the position of the fourth ramp (bleed door 90 percent open) were the $18^\circ + 5^\circ$ combination produced the highest recovery (0.433) and lowest distortion (0.055), the $15^\circ + 13^\circ$ angles bled the least (0.111 total), the $15.37^\circ + 9.58^\circ$ combination captured the maximum flow (0.927) and delivered the most to the engine (0.79), and the dynamic distortion was 0.04 to 0.06 for all three sets of ramp angles.

6. The results of reducing the ramp bleed (fourth ramp set at optimum) were the $18^\circ + 5^\circ$ combination produced the highest recovery (0.441) and the lowest distortion (0.125), the $15.37^\circ + 9.58^\circ$ combination bled the least (0.079 total) and captured the maximum flow (0.892) and delivered the most to the engine (0.812), and the dynamic distortion was 0.04 to 0.06 for all three configurations.

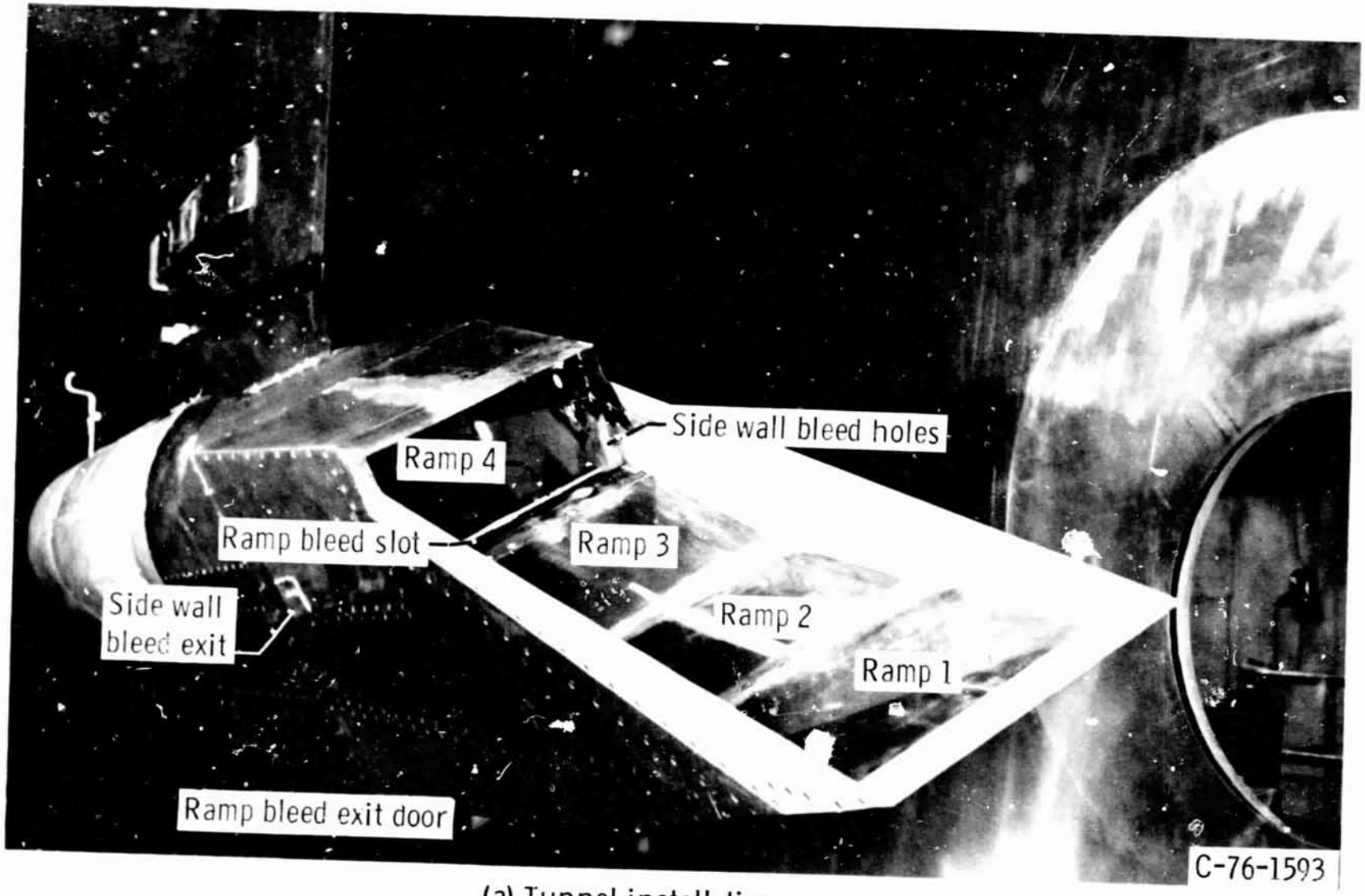

(a) Tunnel installation.

Figure 1. - Model details.

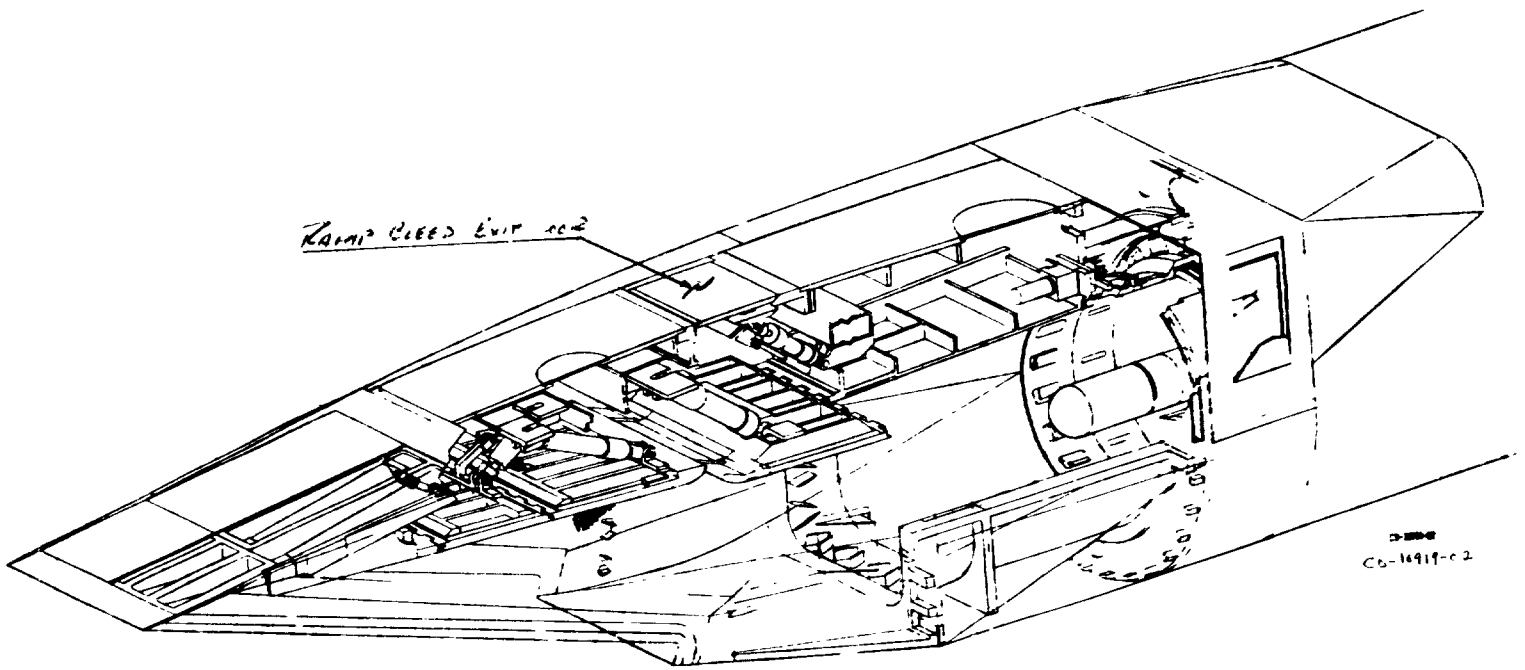

b- SCHEMATIC OF MODEL

FIGURE 1:- CONTINUED

λ_1 = FIXED 3° RAMP

λ_2 = REMOTELY VARIABLE

λ_3 = " "

λ_4 = " " (DOWN = NEGATIVE)

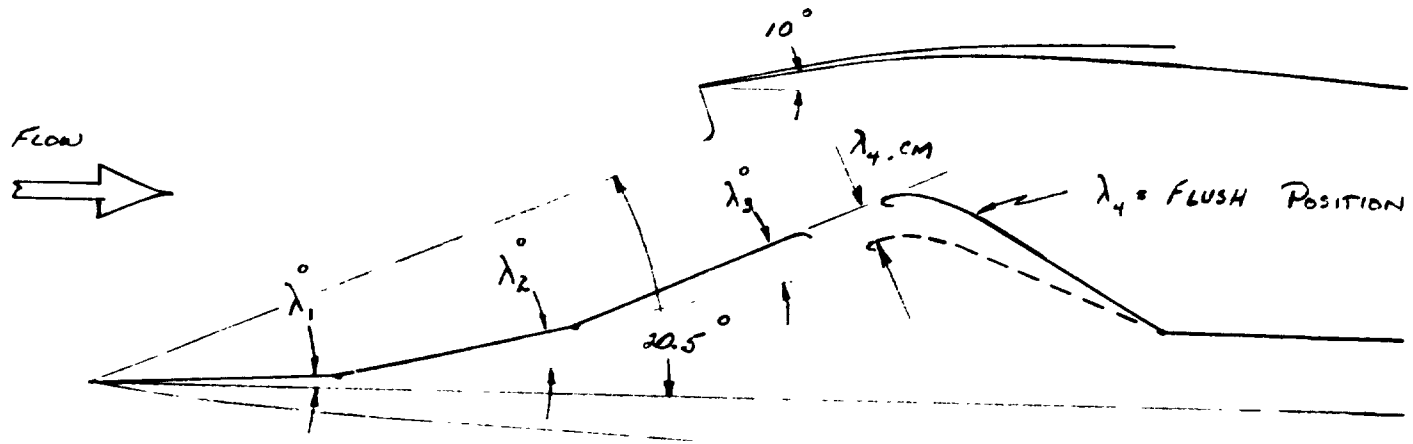

c- DEFINITION OF INLET RAMP POSITIONS FOR 100-0 INLET
(DRAWING NOT TO SCALE)

FIGURE 1: CONCLUDED

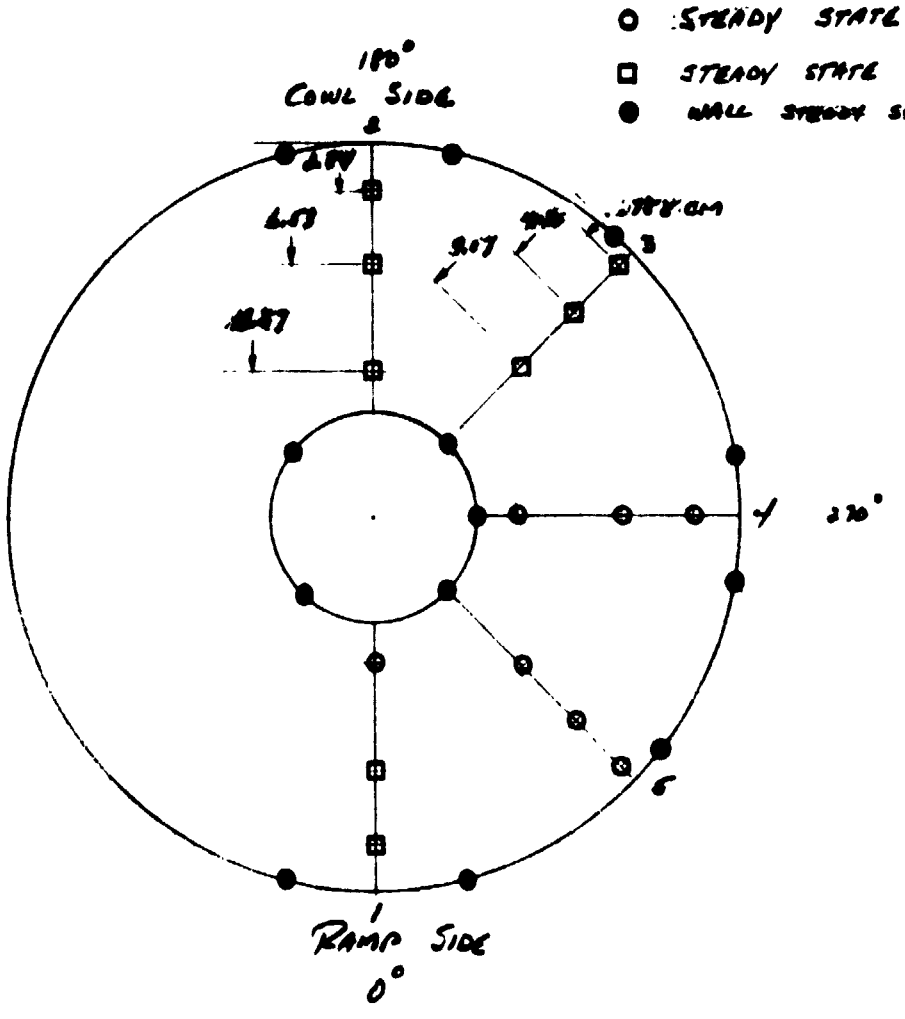

FIGURE:- 2 COMPRESSOR FACE INSTRUMENTATION FOR MACH 3.5 TEST OF 110-0 INLET

	Region 1	2	3	4	5	6	7
M_i	3.5	3.315	2.458	3.5	2.38	3.5	1.7
λ	3°	15.37°	9.58°	18.65°	9.9°	39.3°	19.3°
θ_w	18.65°	30.6°	31.6°	33.2°	33.1°	46.5°	90°
P/P_i	1.3	3.15	1.79	4.085	1.79	7.33	3.205
P/P_o	1.3	4.095	7.33	4.085	7.33	7.33	33.48
M_{out}	3.315	2.458	3.085	2.38	1.99	1.700	.641 (N.S.)
P_i/P_o	.995	.862	.979	.761	.979	.484	
P/P_o	.995	.858	.846		.745		
$P/P_o)_{N.S.}$			.676		.726		.956
$P/P_o)_{C.L.}$			.568		.541		.414
$P/P_o)_{AVG.}$							.508

$\dot{m}/\dot{m}_\infty)_{CAPT} \approx .99$

$P/P_o)_{MEAS.} = 16.27$

P_i/P_o = Local Pressure Recovery (Region)
P/P_o = " " " (Accum)
$P/P_o)_{N.S.}$ = " " " (Normal Shock)
$P/P_o)_{C.L.}$ = " " " (Accum. @ Cowl Lip)

$P/P_o)_{AVG.}$ = Arithmetic Avg. Across Entire Cowl Lip Sta.

——— Ramp Surface or oblique shock
— — — Sidefairing
----- Slip Lines from shock intersection

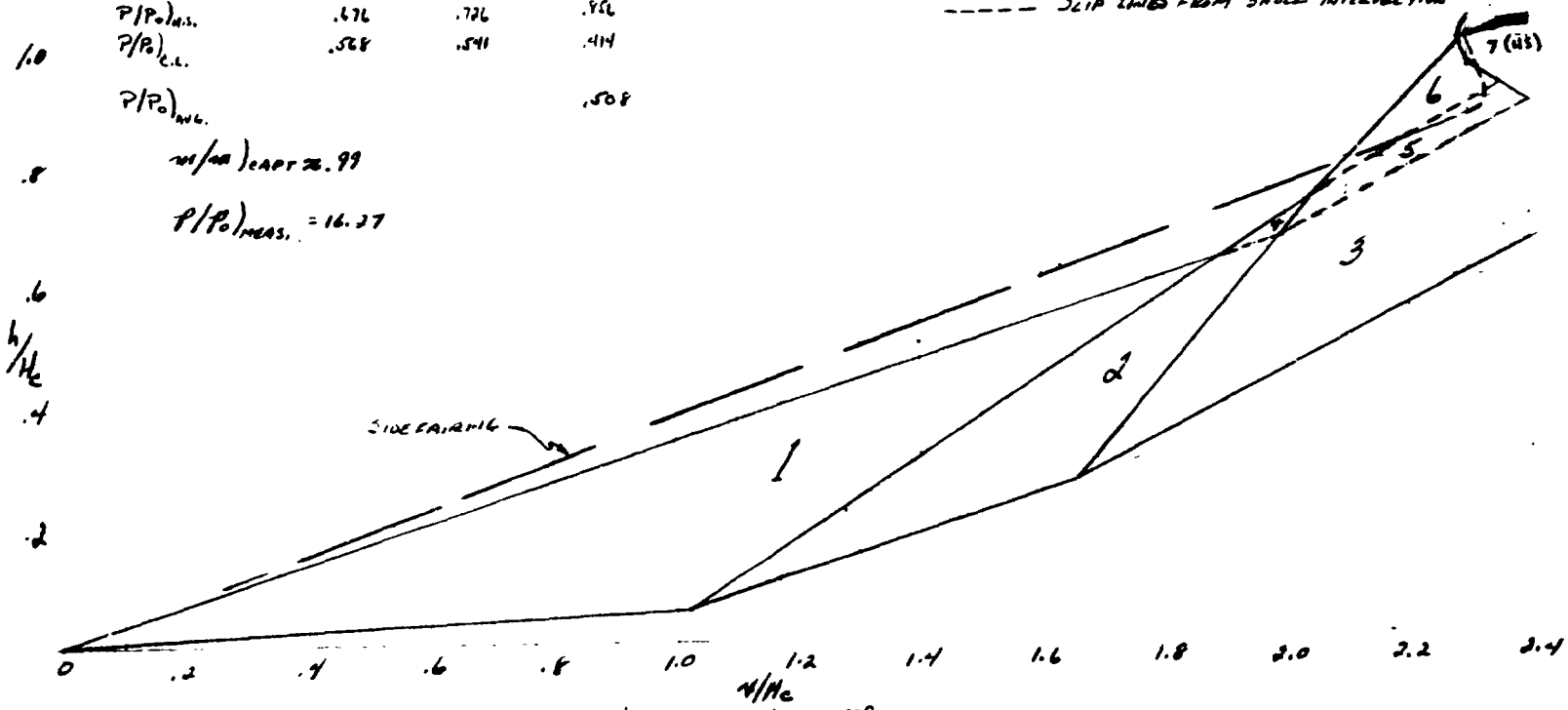

a - $\lambda_1 = 3°$, $\lambda_2 = 15.37°$, $\lambda_3 = 9.58°$

Figure 3 - Theoretical Shock Patterns at Mach 3.5

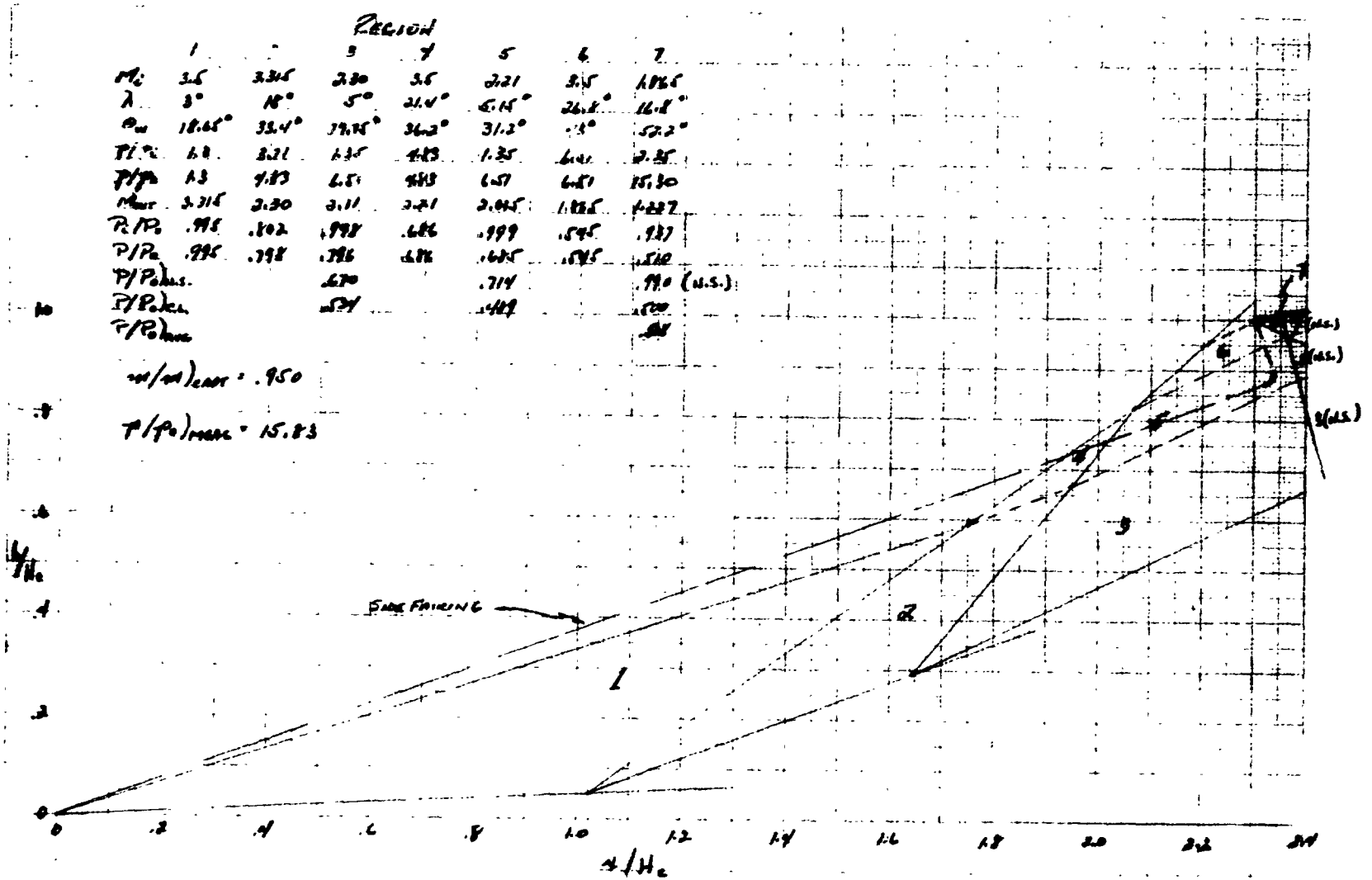

FIGURE 3- CONTINUED,

6- $\lambda_1 = 3°$, $\lambda_2 = 18°$, $\lambda_3 = 5°$

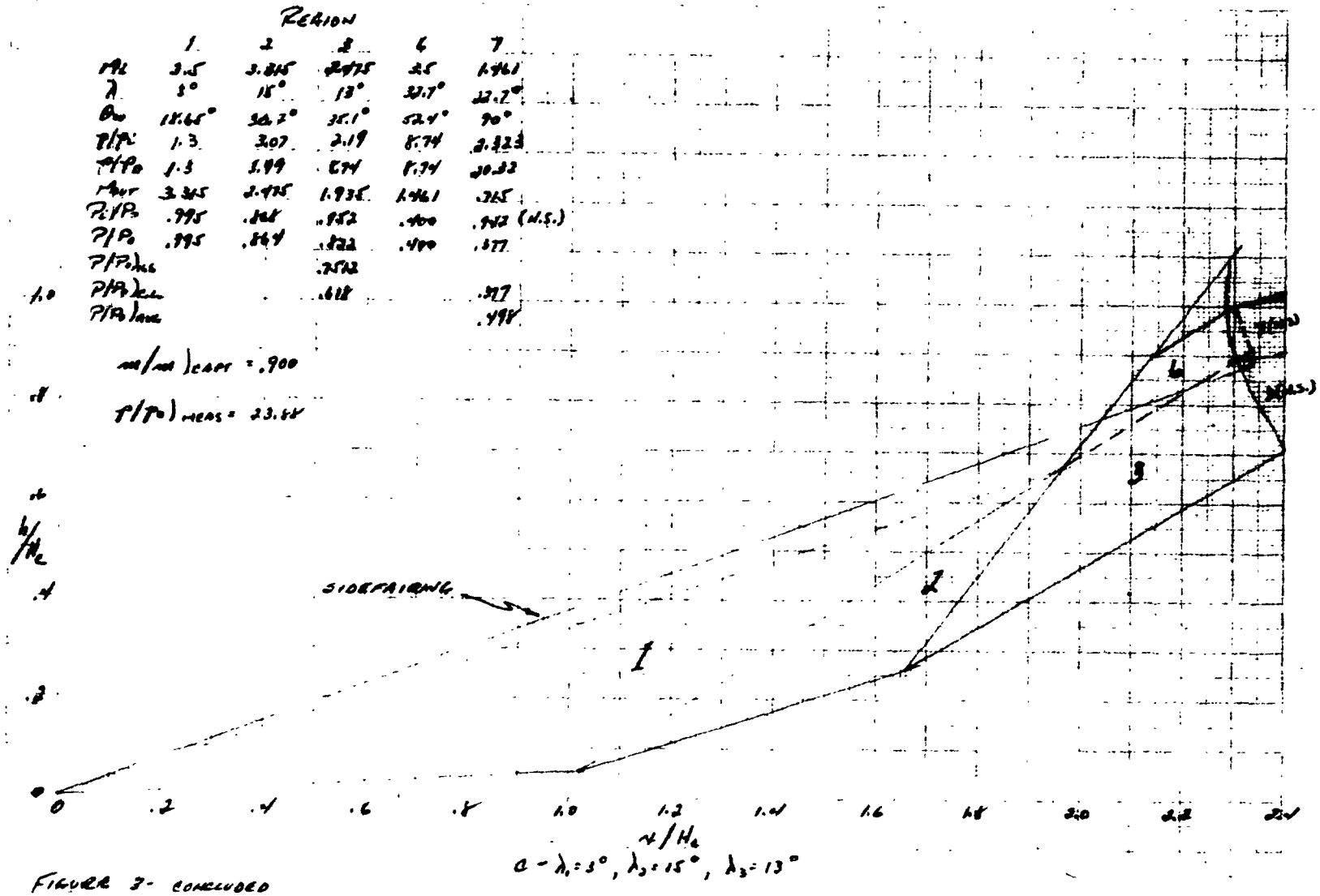

FIGURE 3- CONCLUDED

Run 35
Pages 22-26

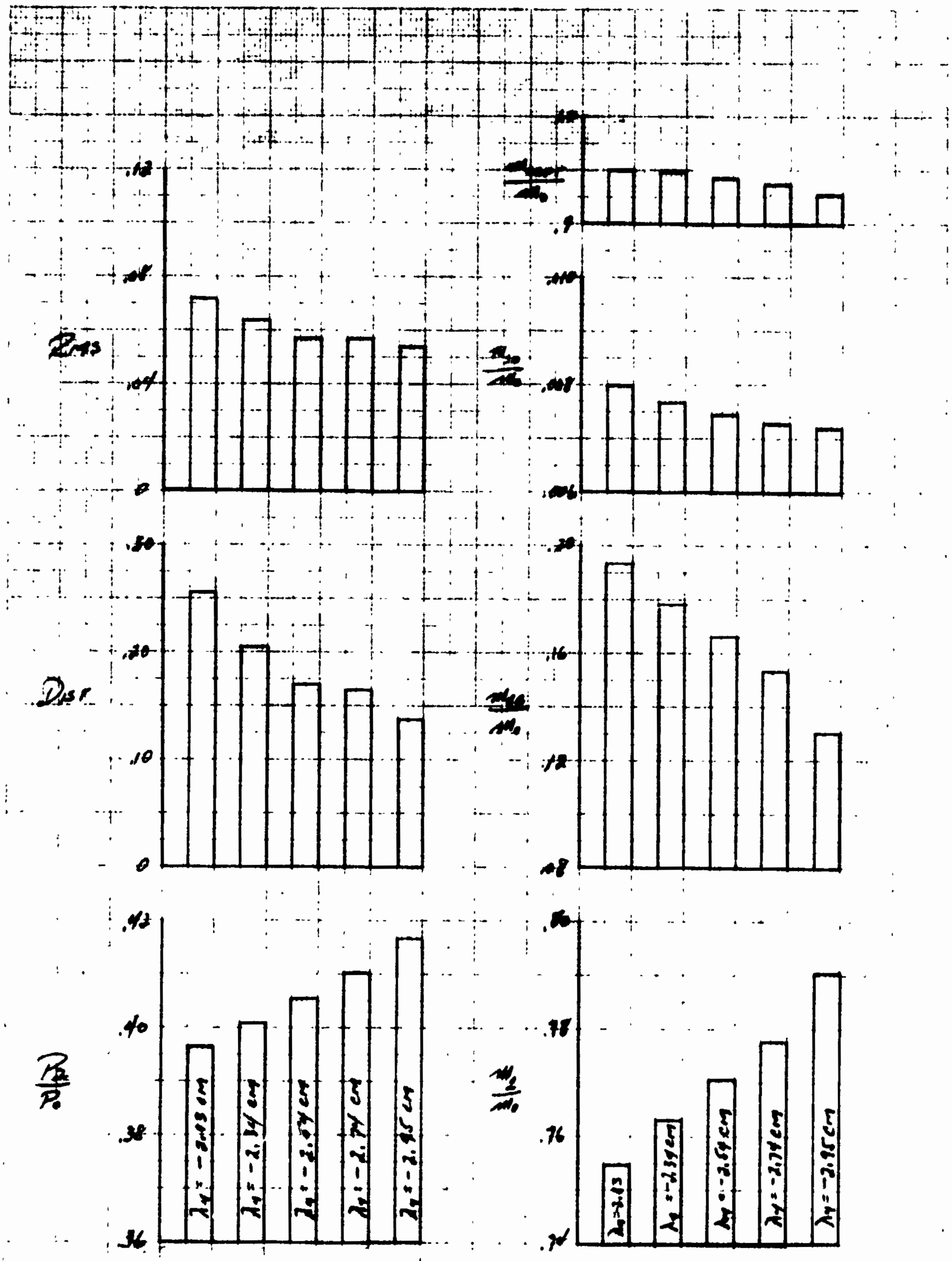

$\lambda_1 = 3^\circ$, $\lambda_2 = 15.89^\circ$, $\lambda_3 = 9.55^\circ$, [illegible]

FIGURE 4 - EFFECT OF [illegible] RAMP HEIGHT ON OPTIMAL INLET PERFORMANCE AT [illegible]

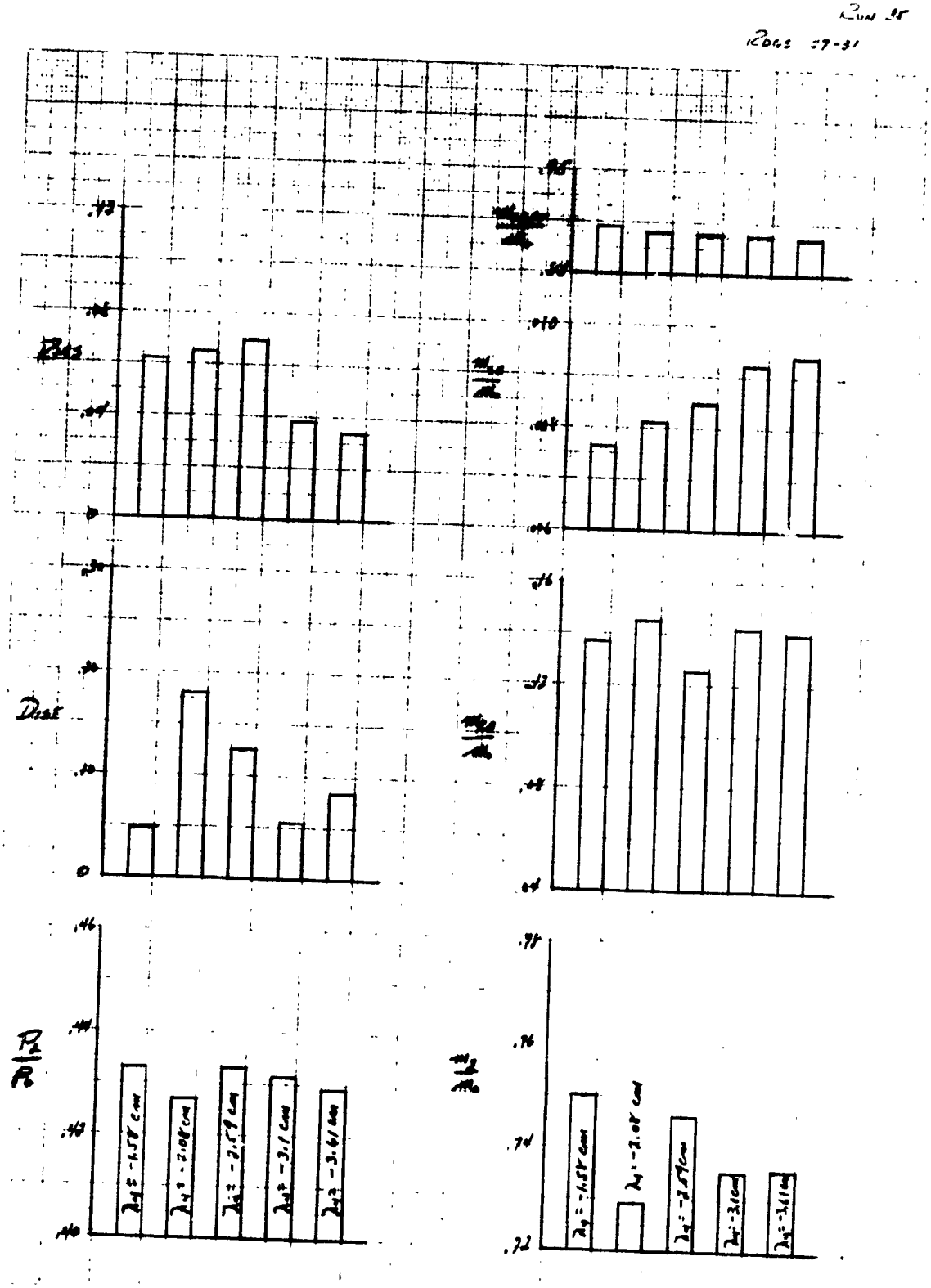

Figure 4 - Continued, 6- $\lambda_1 = 1°$, $\lambda_3 = 11°$, $\lambda_5 = 5°$, w(rad/s) = 0.524 sign/sec

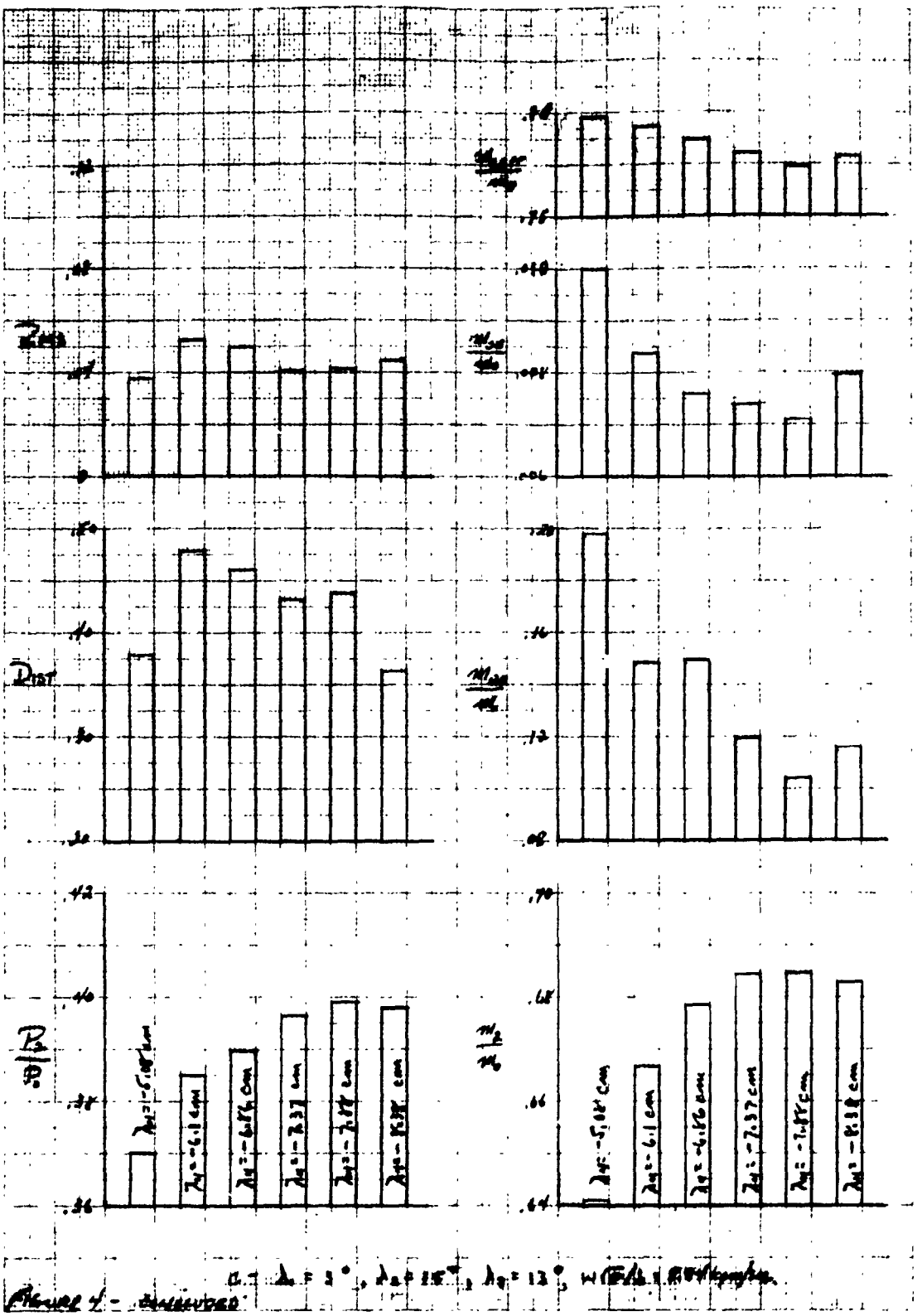

Figure 4 - [illegible] a: $\lambda_1 = 5°$, $\lambda_2 = 15°$, $\lambda_3 = 13°$, [illegible]

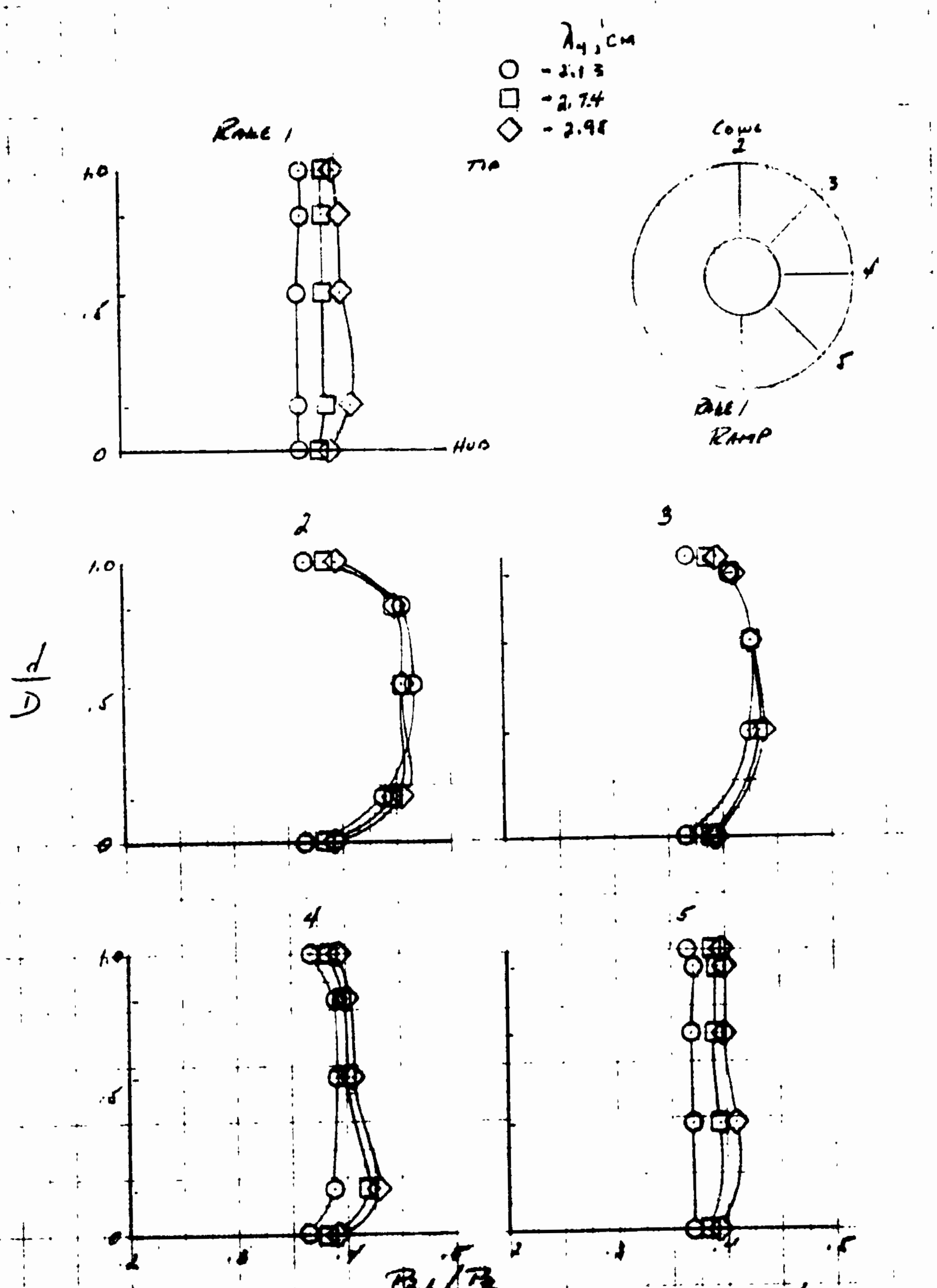

$a - \lambda_1 = 3^\circ, \lambda_2 = 45.37^\circ, \lambda_3 = 9.58^\circ, w\sqrt{\theta}/\delta = 2.85$ kg/sec.

Figure 5 Effect of [illegible] Ramp Position on Compressor Face Steady State Total Pressure Profiles at [illegible]

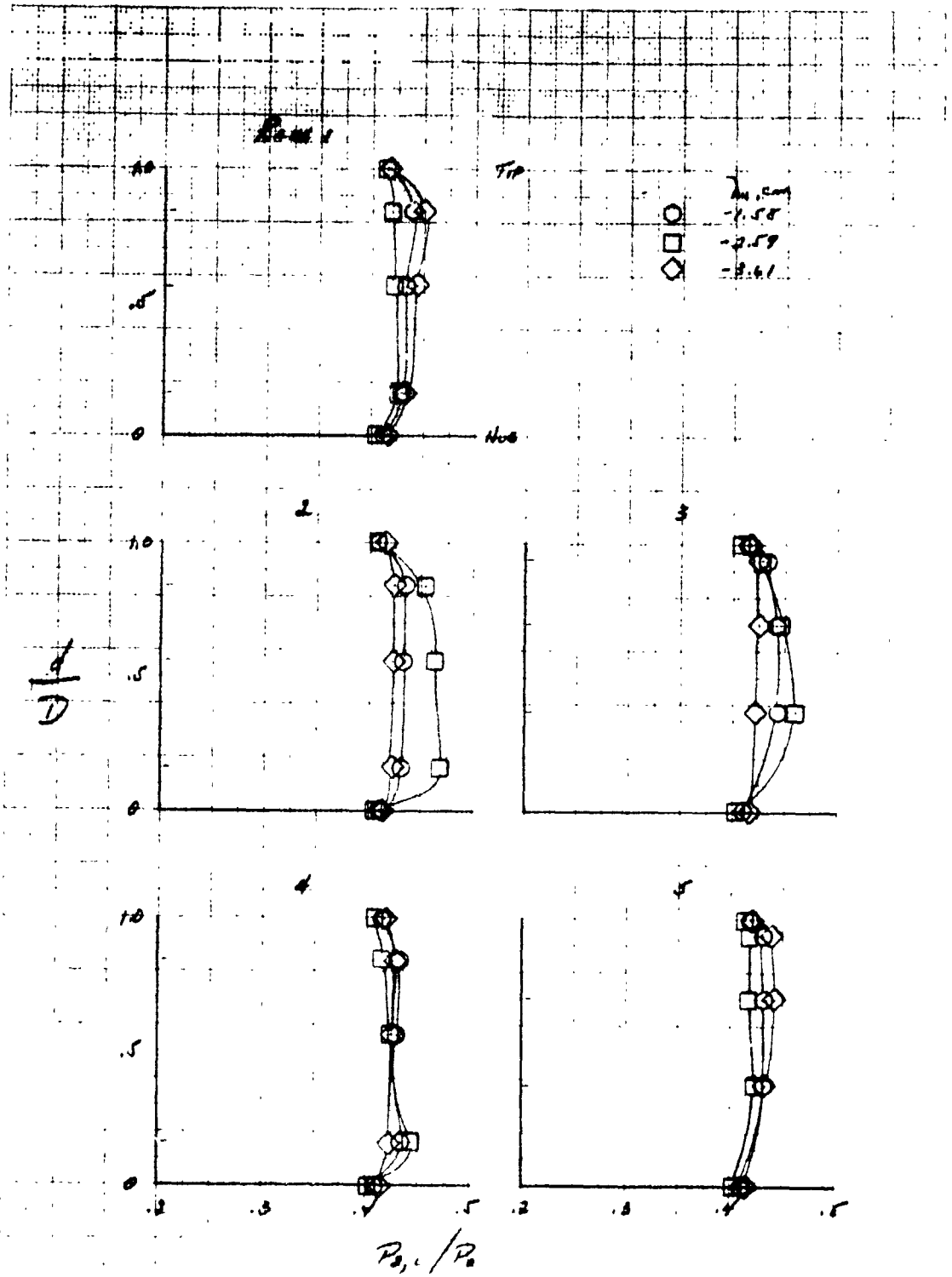

FIGURE 5 CONTINUED 6- $\lambda_1 = 5°$, $\lambda_2 = 18°$, $\lambda_3 = 5°$, $\omega r_0/a = 8.94$ kgm/sec.

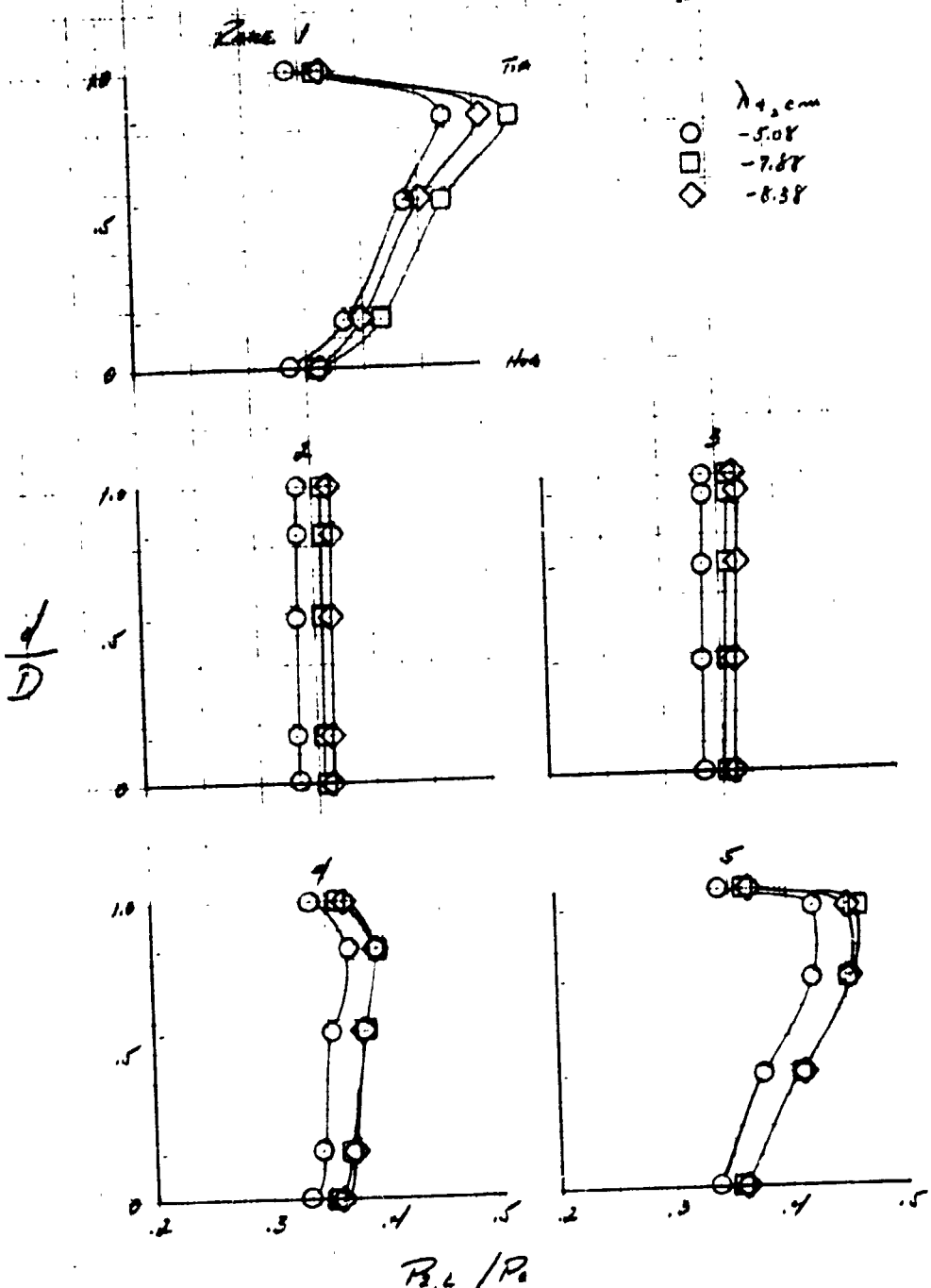

c- $\lambda_1 = 3°$, $\lambda_2 = 15°$, $\lambda_3 = 13°$, $\omega r/\delta = 8.94$ kgm/sec

FIGURE 5 . CONCLUDED

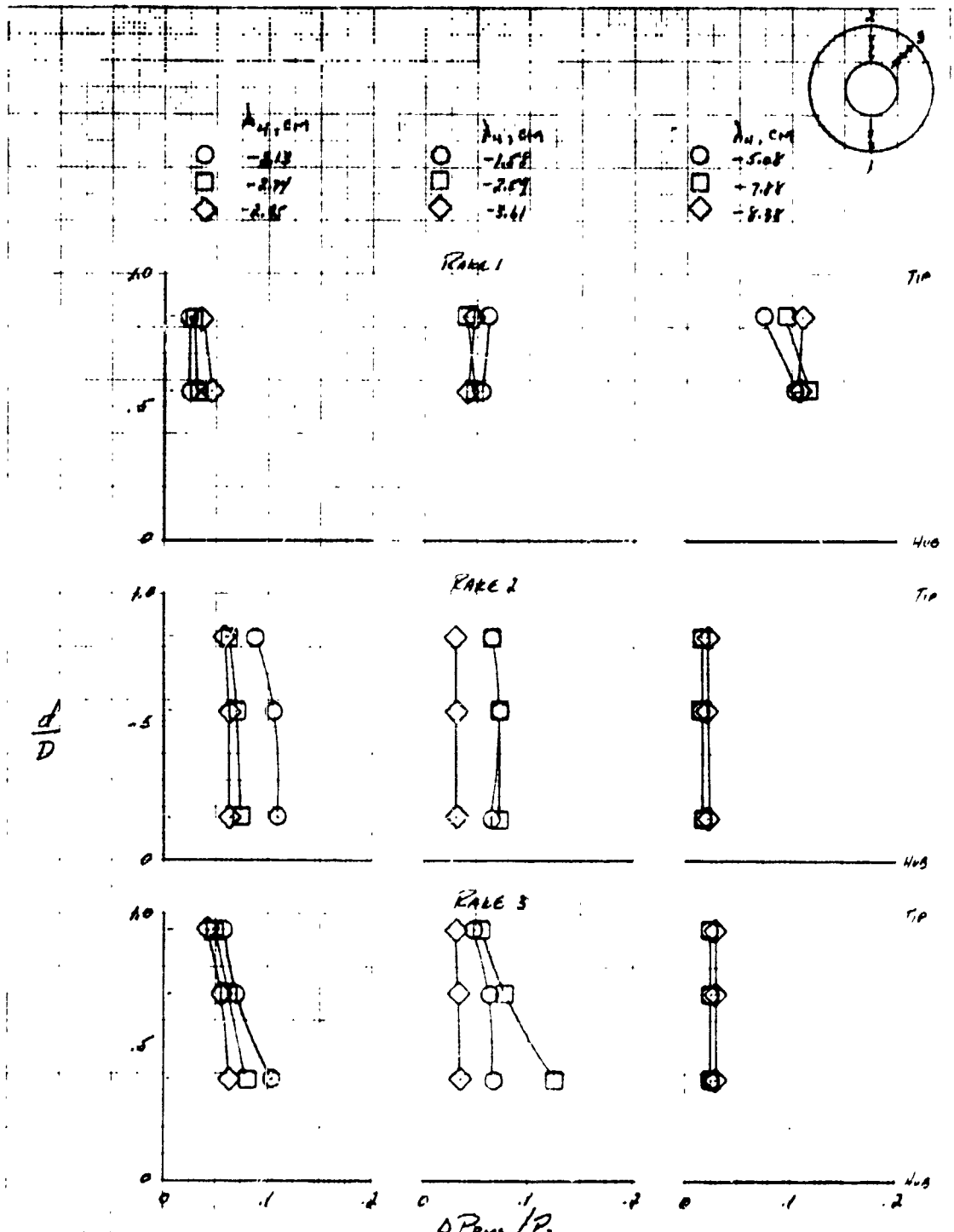

FIGURE 6 EFFECT OF FOURTH RAMP POSITION ON COMPRESSOR FACE DYNAMIC TOTAL PRESSURE PROFILES AT $M_0 = 2.5$, $Re = 2.05 \times 10^6$/cm, $\alpha = \beta = 0°$, $\beta_c = 90\%$

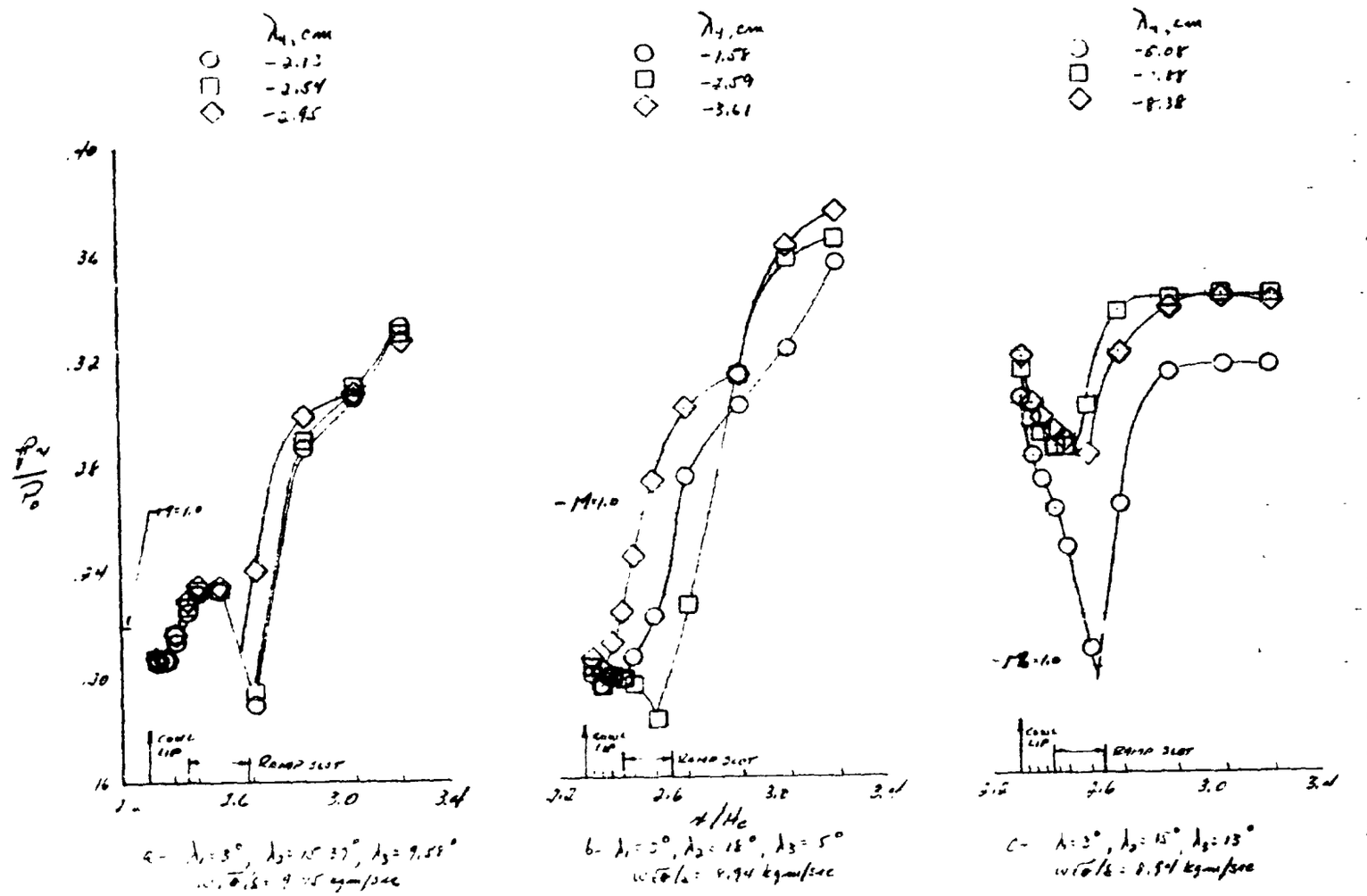

a- $\lambda_1 = 3°$, $\lambda_2 = 15°$ 33', $\lambda_3 = 9.58°$
$\dot{w}\sqrt{\theta}/\delta = 9.45$ kg-m/sec

b- $\lambda_1 = 3°$, $\lambda_2 = 18°$, $\lambda_3 = 5°$
$\dot{w}\sqrt{\theta}/\delta = 9.94$ kg-m/sec

c- $\lambda_1 = 3°$, $\lambda_2 = 15°$, $\lambda_3 = 13°$
$\dot{w}\sqrt{\theta}/\delta = 8.54$ kg-m/sec

FIGURE 7 - EFFECT OF FOURTH RAMP POSITION ON COWL PRESSURE DISTRIBUTIONS, $M_\infty = 2.5$, $Re = 2.5 \times 10^6$/m, $\alpha = \beta = 0°$, $\delta\beta = 90\%$

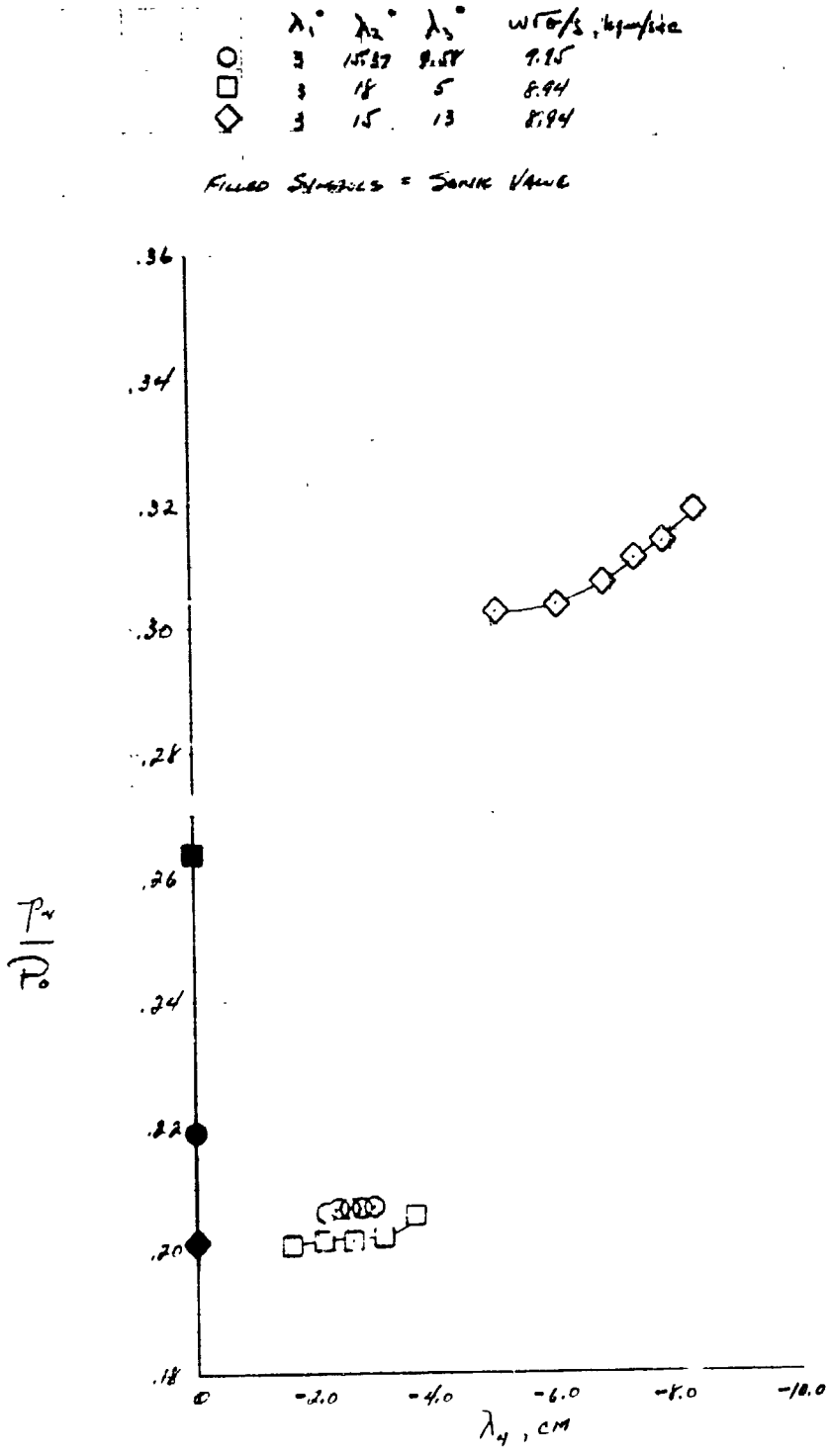

FIGURE 8 - EFFECT OF FOURTH RAMP POSITION ON COWL LIP STATIC PRESSURE AT $M_0 = 3.52$, $Re = 7.05 \times 10^6/m$, $\alpha = \beta = 0°$, BL = 90%

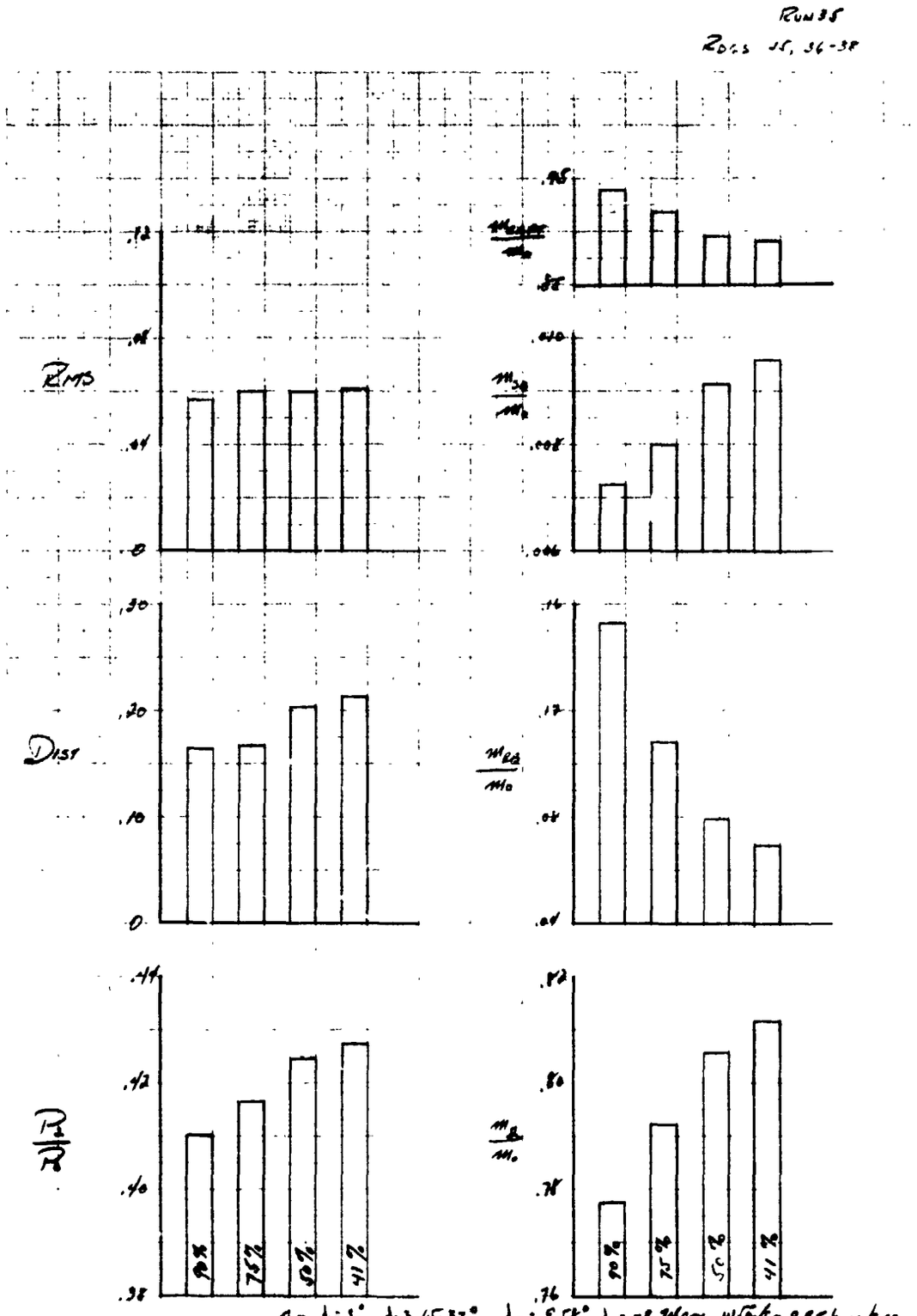

a - $\lambda_1 = 3°$, $\lambda_2 = 15.37°$, $\lambda_3 = 9.58°$, $\lambda_4 = -2.74$ cm, $w\sqrt{\theta}/\beta = 9.95$ ft, $\sqrt{\text{sec}}$.

FIGURE 9 - EFFECT OF BLEED DOOR POSITION ON CRITICAL INLET PERFORMANCE AT $M_\infty = 3.58$, $Re = 1.05 \times 10^6/\text{in}$, $\alpha = \beta = 0$.

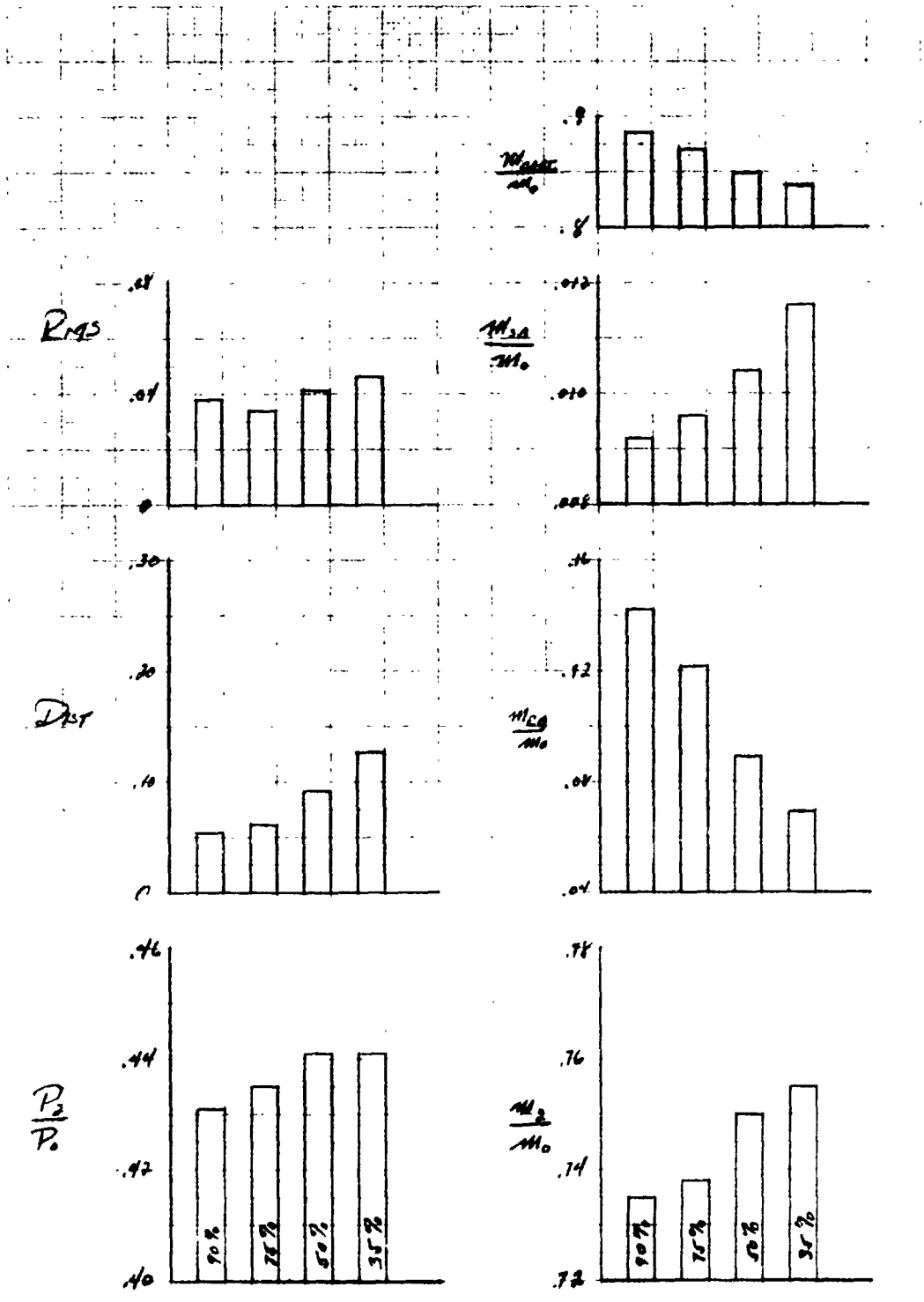

b- $\lambda_1 = 3°$, $\lambda_2 = 18°$, $\lambda_3 = 5°$, $\lambda_4 = -8.1$ cm, $\omega\sqrt{\theta}/k = 8.34$ kg-m/sec

FIGURE 9 - CONTINUED,

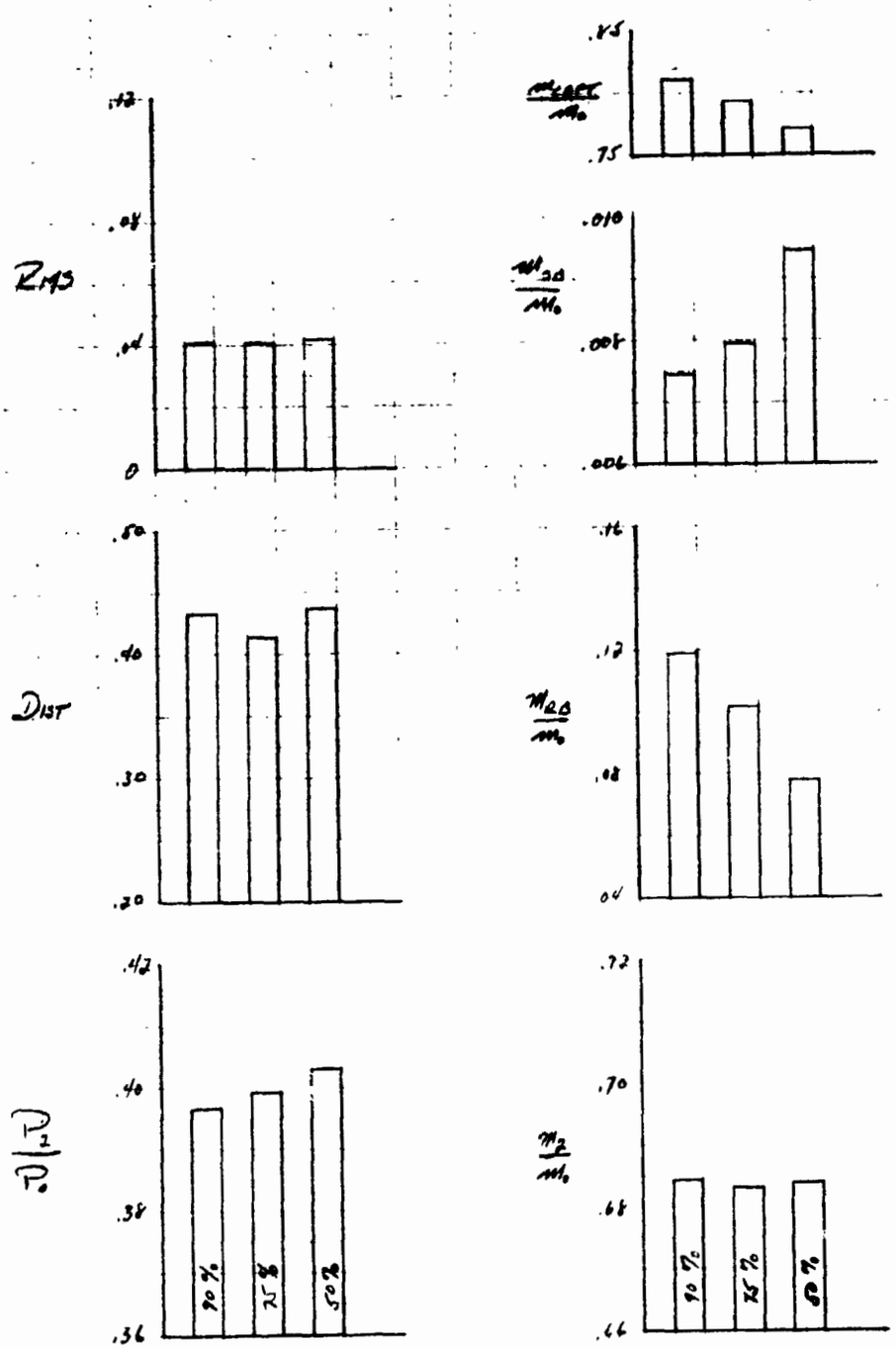

C- $\lambda_1 = 3°$, $\lambda_2 = 15°$, $\lambda_3 = 13°$, $\lambda_4 = -7.37$ cm, $W/\sqrt{\theta}/\delta = 8.94$ kg/sec/sec

FIGURE 9- CONCLUDED.

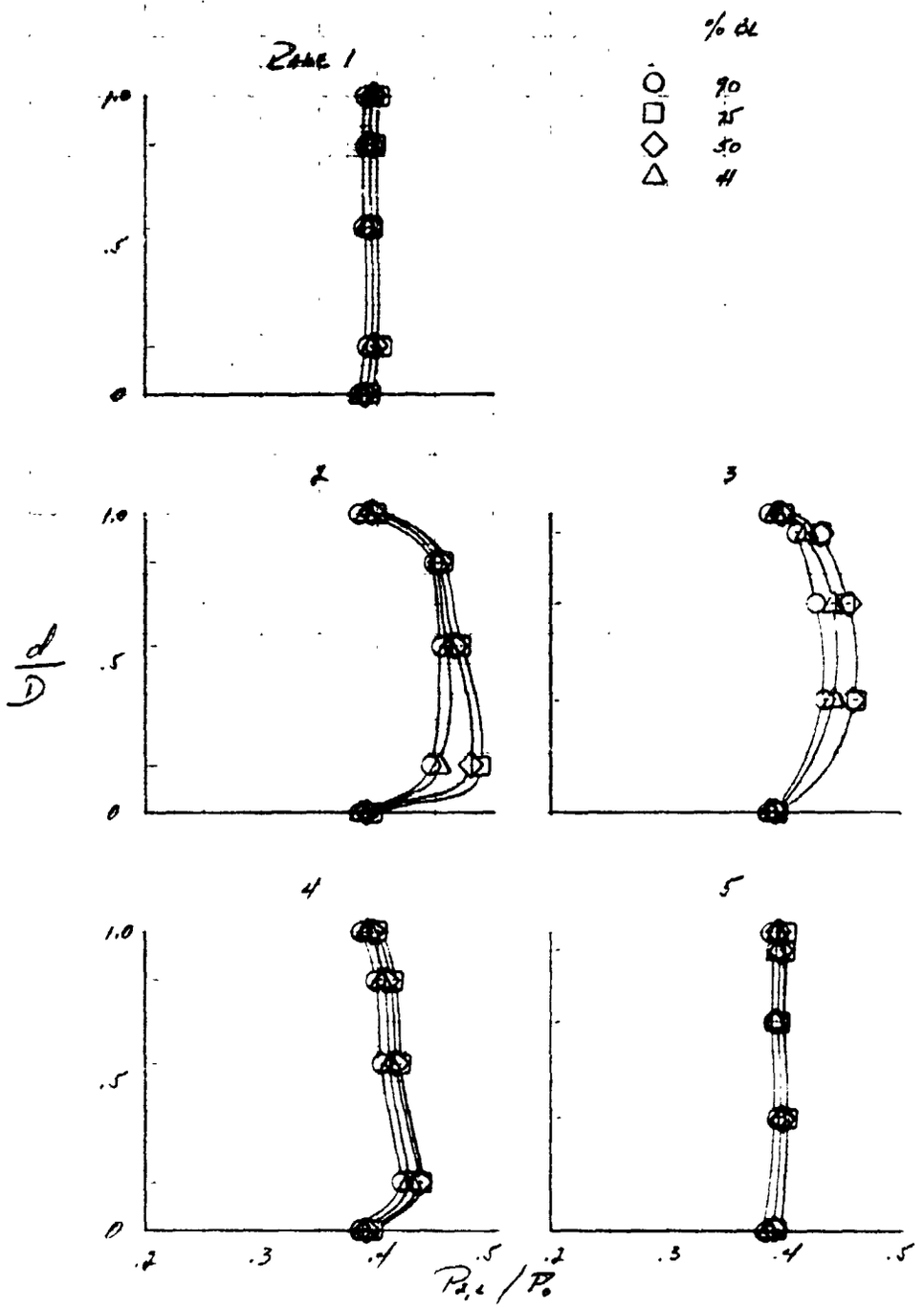

a - $\lambda_1 = 8°$, $\lambda_2 = 15.37°$, $\lambda_3 = 9.58°$, $\lambda_N = -2.79$ cm, $w/\theta/\delta = 9.95$ kg/m/sec

FIGURE 10 - EFFECT OF BLEED DOOR POSITION ON COMPRESSOR FACE STEADY STATE TOTAL PRESSURE PROFILES AT $M_0 = 3.52$, $Re = 7.05 \times 10^6$/m, $\alpha = \beta = 0°$

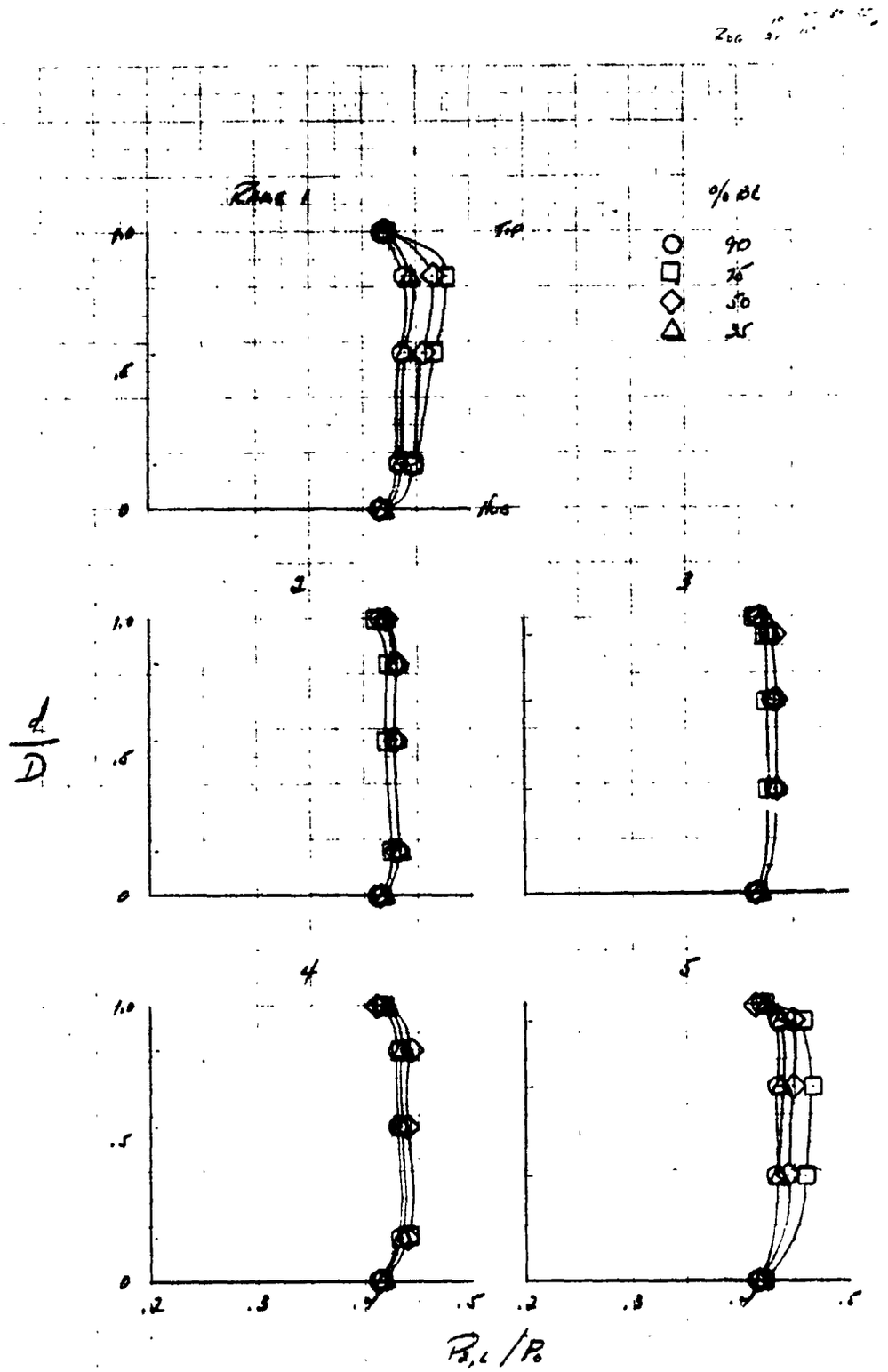

6- $\lambda_1 = 3°$, $\lambda_2 = 18°$, $\lambda_3 = 5°$, $\lambda_y = -3.1$ cm, $W\sqrt{\theta}/\delta = 5.94$ kgm/sec

Figure 19 - CONTINUED.

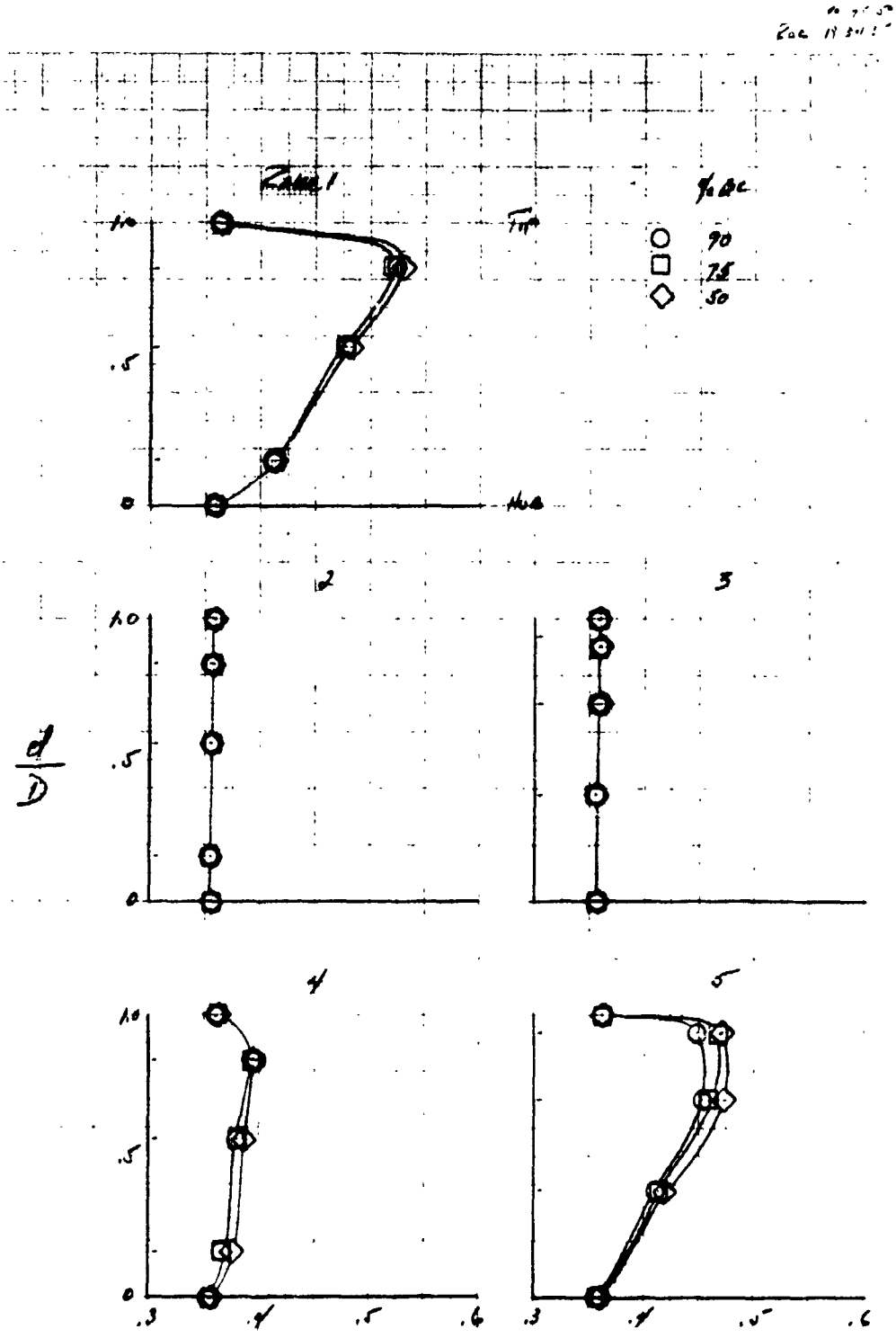

c- $\lambda_1 = 3°$, $\lambda_2 = 15°$, $\lambda_3 = 13°$, $\lambda_4 = -7.37$ cm, $w_{\dot{m}/s} = 8.94$ kg/m/sec

FIGURE 10. CONCLUDED.

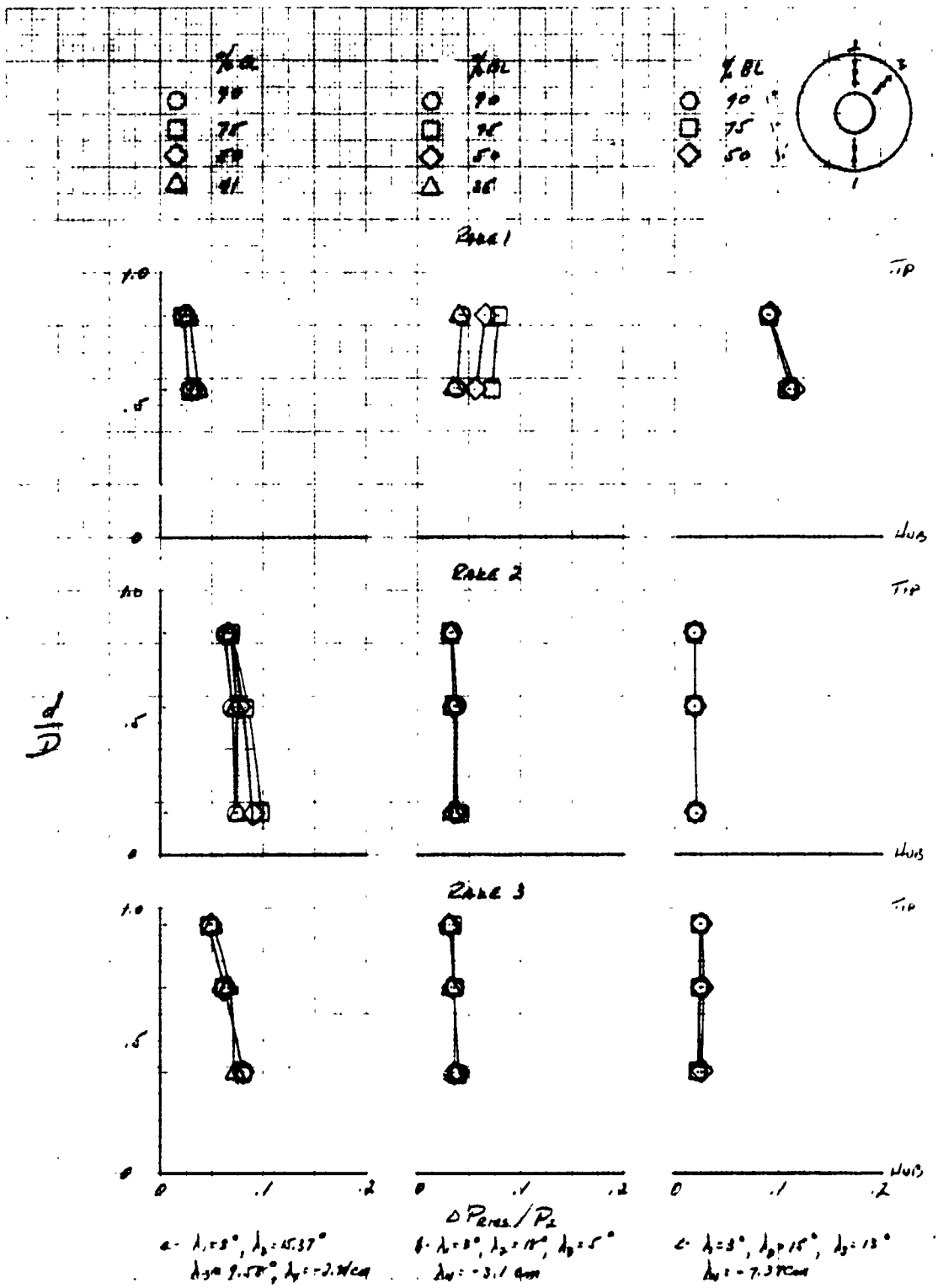

a- $\lambda_1 = 3°$, $\lambda_2 = 45.37°$
$\lambda_3 = 9.58°$, $\lambda_4 = -2.1$ cm

b- $\lambda_1 = 3°$, $\lambda_2 = 18°$, $\lambda_3 = 5°$
$\lambda_4 = -3.1$ cm

c- $\lambda_1 = 3°$, $\lambda_2 = 15°$, $\lambda_3 = 13°$
$\lambda_4 = -7.3$ cm

FIGURE 11 EFFECT OF BLEED DOOR OPENING ON COMPRESSOR EXIT DYNAMIC TOTAL PRESSURE PROFILES AT $M_2 = 3.52$, $R_{e_2} = 7.05 \times 10^6$/ft, $\alpha_2 = 0°$

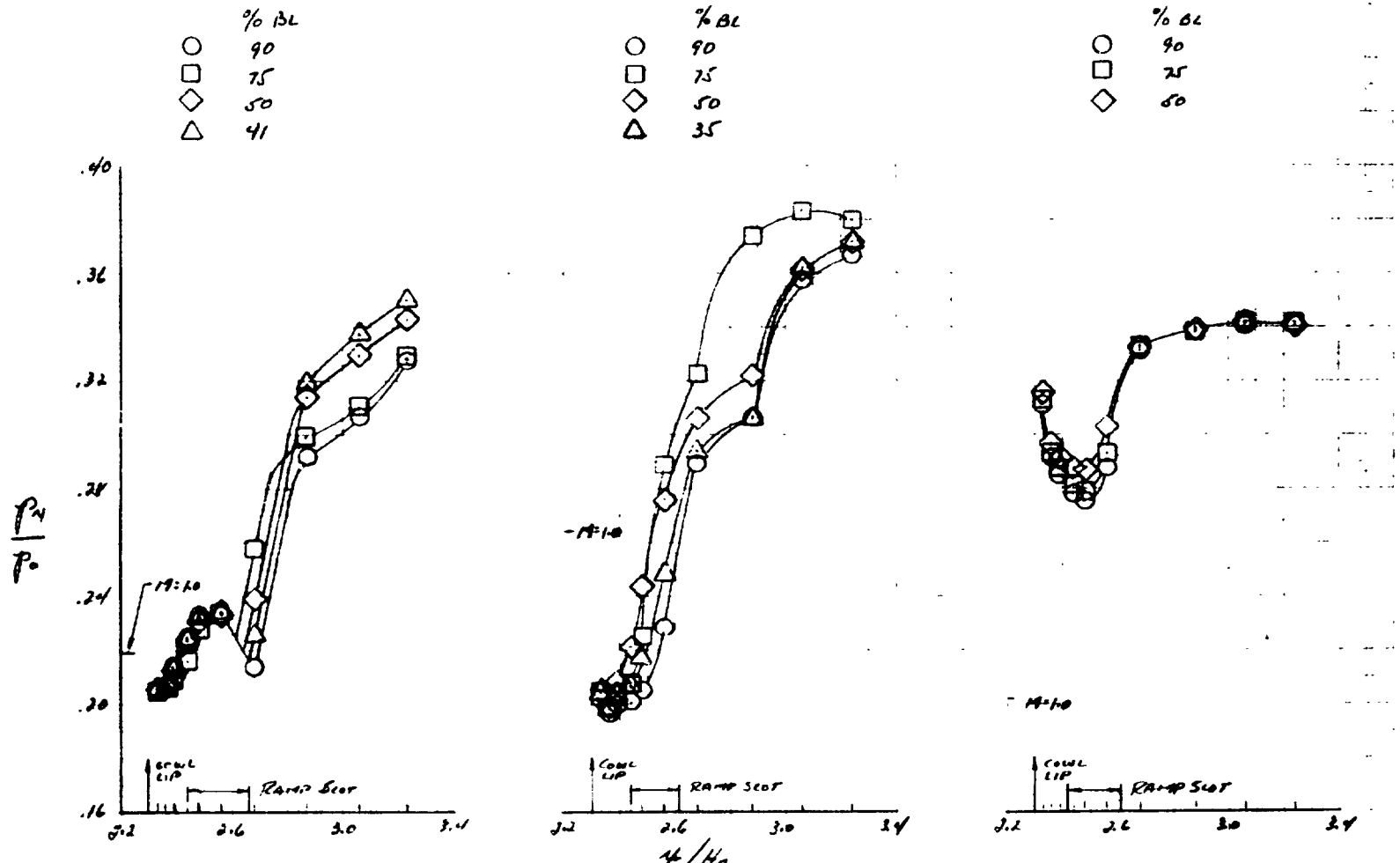

a- $\lambda_1 = 3°$, $\lambda_2 = 15.37°$, $\lambda_3 = 9.58°$, $\lambda_4 = -2.74$ cm, $w\sqrt{\theta}/\delta = 9.95$ kg-m/sec

b- $\lambda_1 = 3°$, $\lambda_2 = 11°$, $\lambda_3 = 5°$, $\lambda_4 = -3.4$ cm, $w\sqrt{\theta}/\delta = 8.54$ kg-m/sec.

c- $\lambda_1 = 3°$, $\lambda_2 = 15°$, $\lambda_3 = 13°$, $\lambda_4 = -7.37$ cm, $w\sqrt{\theta}/\delta = 8.94$ kg-m/sec

FIGURE 12 EFFECT OF BLEED DOOR POSITION ON COWL PRESSURE DISTRIBUTIONS, $M_0 = 3.52$, $RE = 7.05 \times 10^6$/cm, $\alpha = \beta = 0°$.

	λ_1°	λ_2°	λ_3°	λ_4 cm	$w\sqrt{\theta}/\delta$, kg-m/sec
○	5	16.57	9.58	-2.19	7.95
□	3	14	6	-3.1	7.94
◇	2	14	13	-7.37	7.94

FILLED SYMBOLS = SONIC VALVE

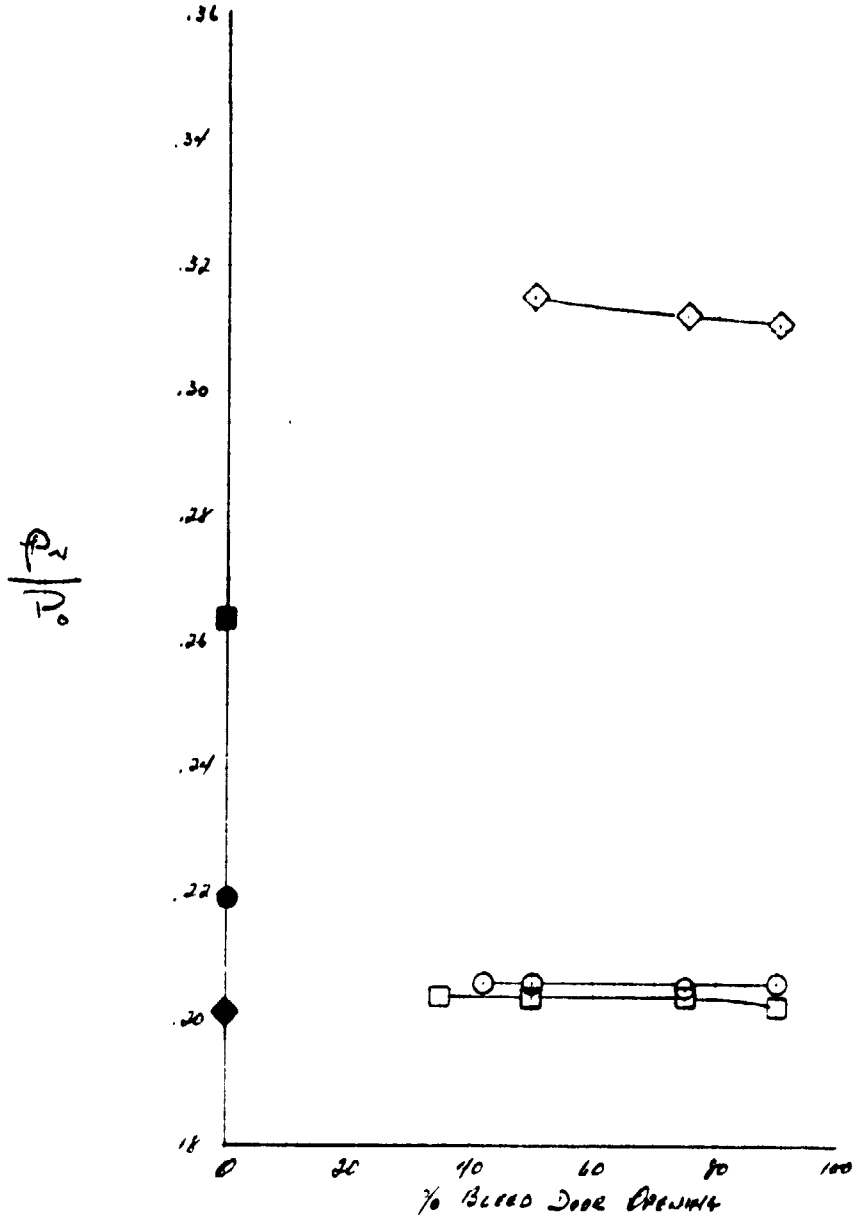

FIGURE 13 - EFFECT OF BLEED DOOR OPENING ON CONE LIP STATIC PRESSURE AT M_0 = 3.52, $Re = 7.05 \times 10^6$/m, $\alpha = \beta = 0°$

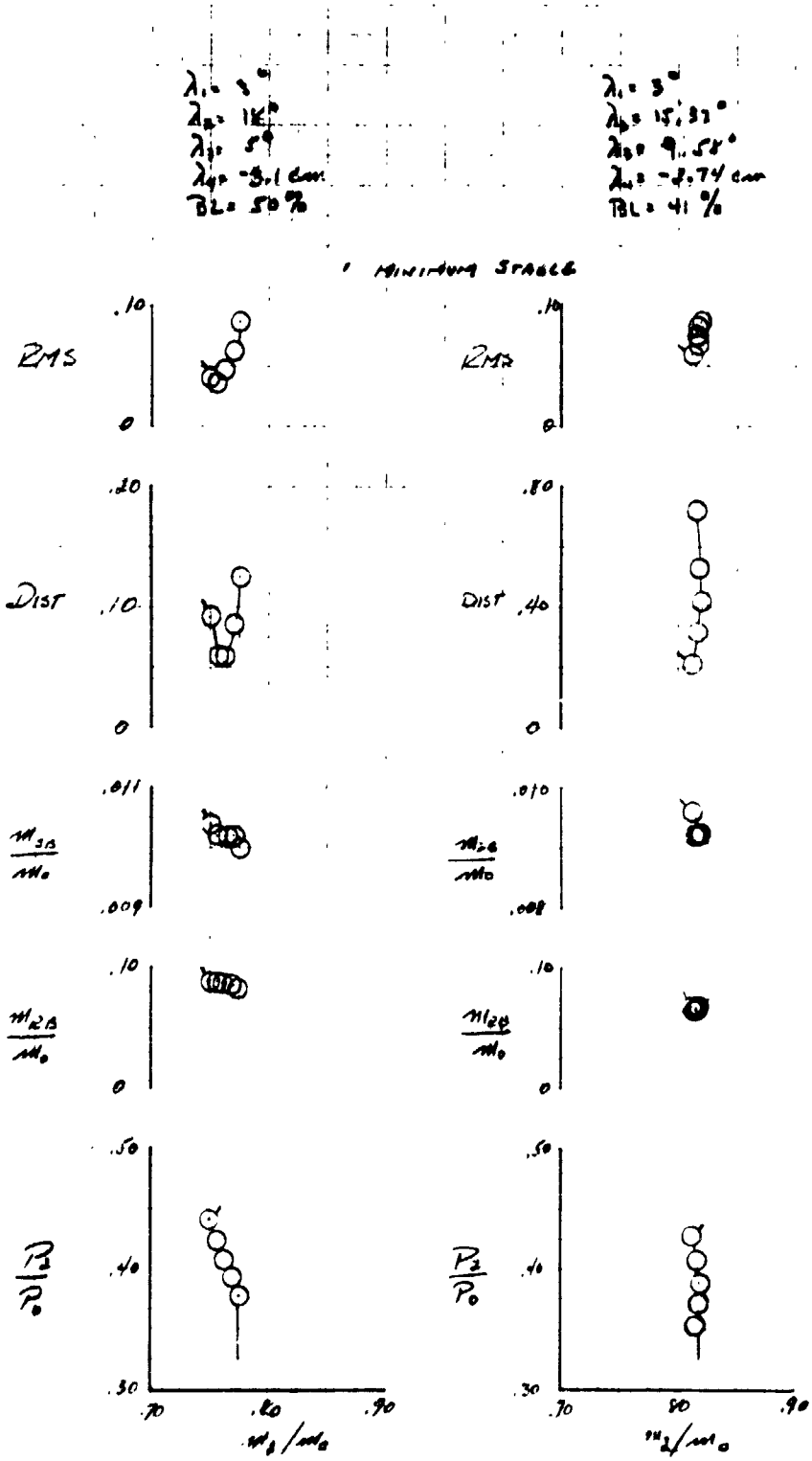

FIGURE 44. INLET PERFORMANCE MAPS AT $M_0 = 3.62$, $R_c = 2.05 \times 10^6$/ft, $\delta = \beta = 0°$.

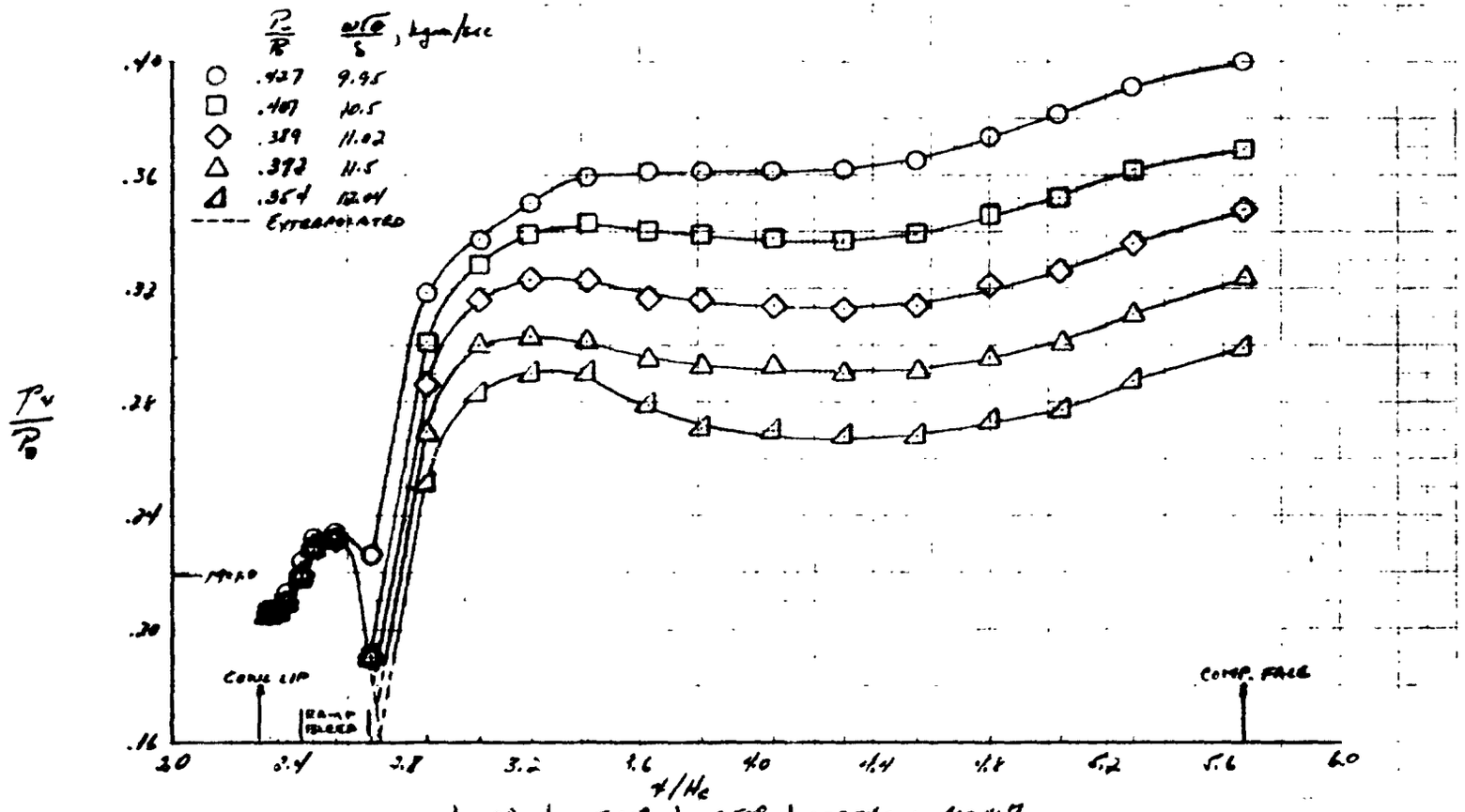

$\alpha - \lambda_1 = 3°$, $\lambda_2 = 15.37°$, $\lambda_3 = 9.58°$, $\lambda_4 = -2.74$ cm, $BL = 41\%$

FIGURE 15 - INTERNAL COWL STATIC PRESSURE DISTRIBUTIONS AT $M_0 = 3.52$, $Re = 7.05 \times 10^6$/cm, $\alpha = \beta = 0°$.

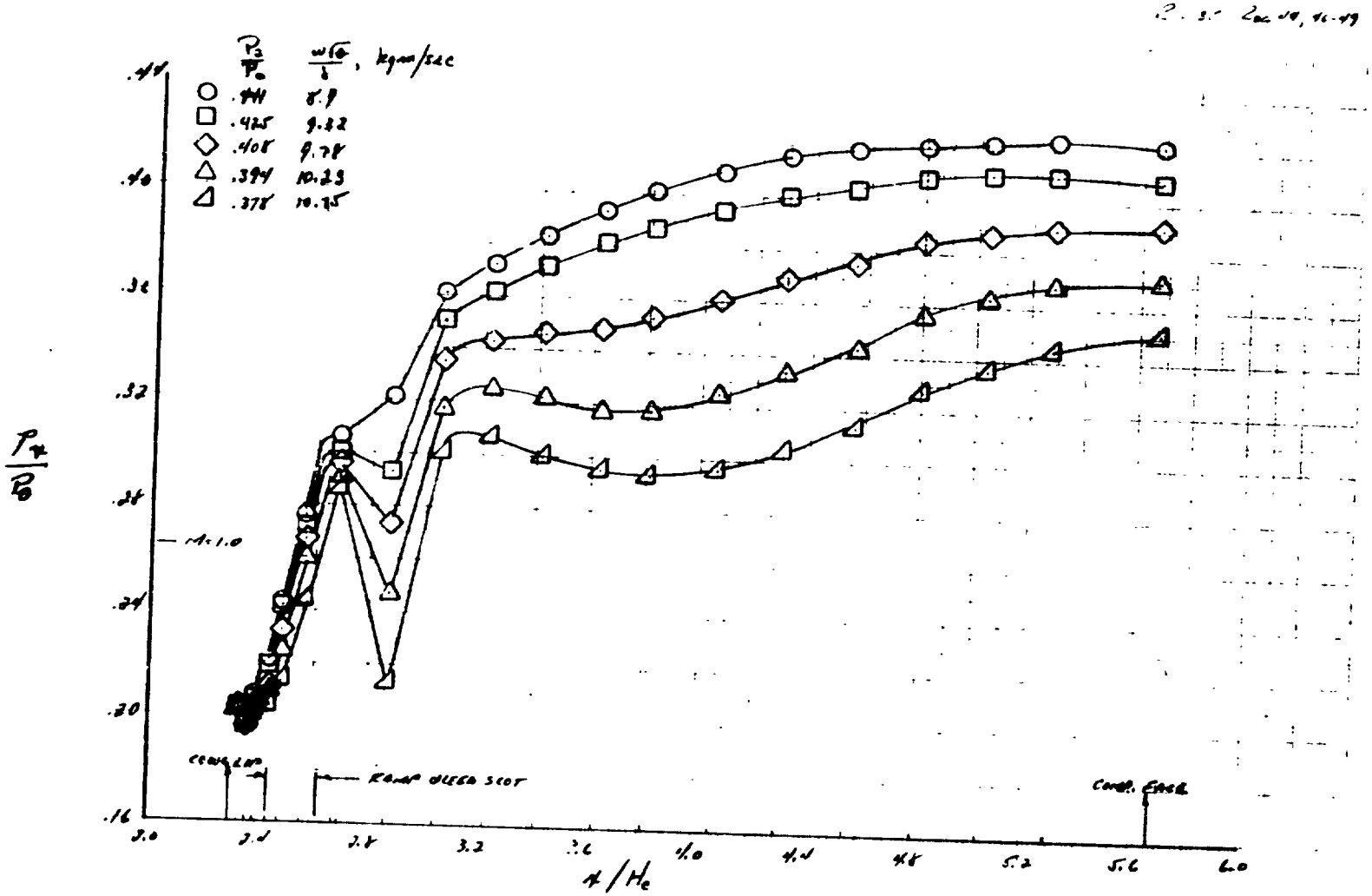

b - $\lambda_1 = 3°$, $\lambda_2 = 16°$, $\lambda_3 = 5°$, $\lambda_4 = -3.1$ cm, BL = 50%

FIGURE 15- CONCLUDED.

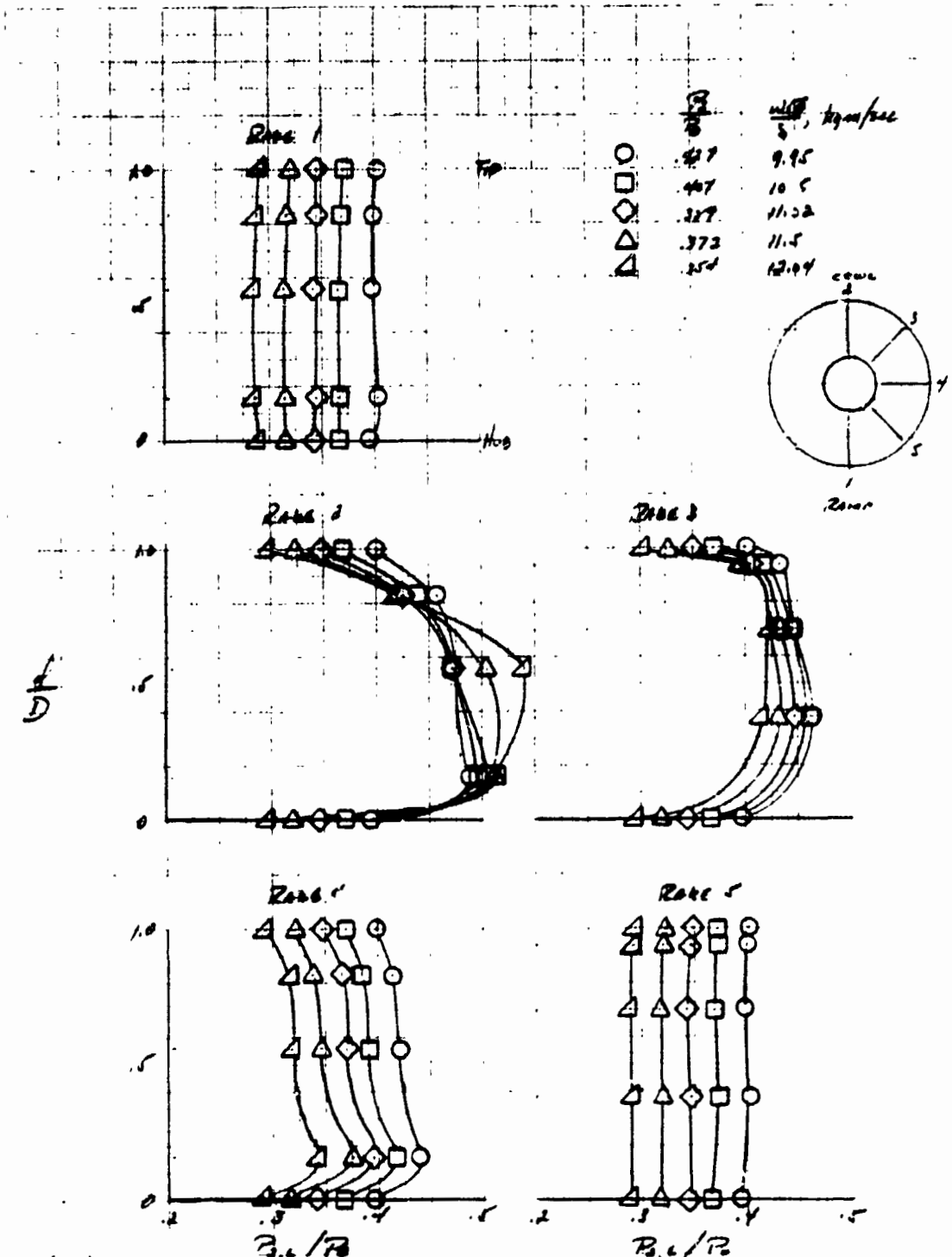

a- $\lambda_1 = 8°$, $\lambda_3 = 47.37°$, $\lambda_5 = 9.58°$, $\lambda_4 = -2.74$ cm, BL = 41%

FIGURE 16- COMPRESSOR FACE STEADY STATE TOTAL PRESSURE PROFILES AT $M_0 = 3.52$, $Re = 2.05 \times 10^6$/m, $\alpha = \beta = 0°$.

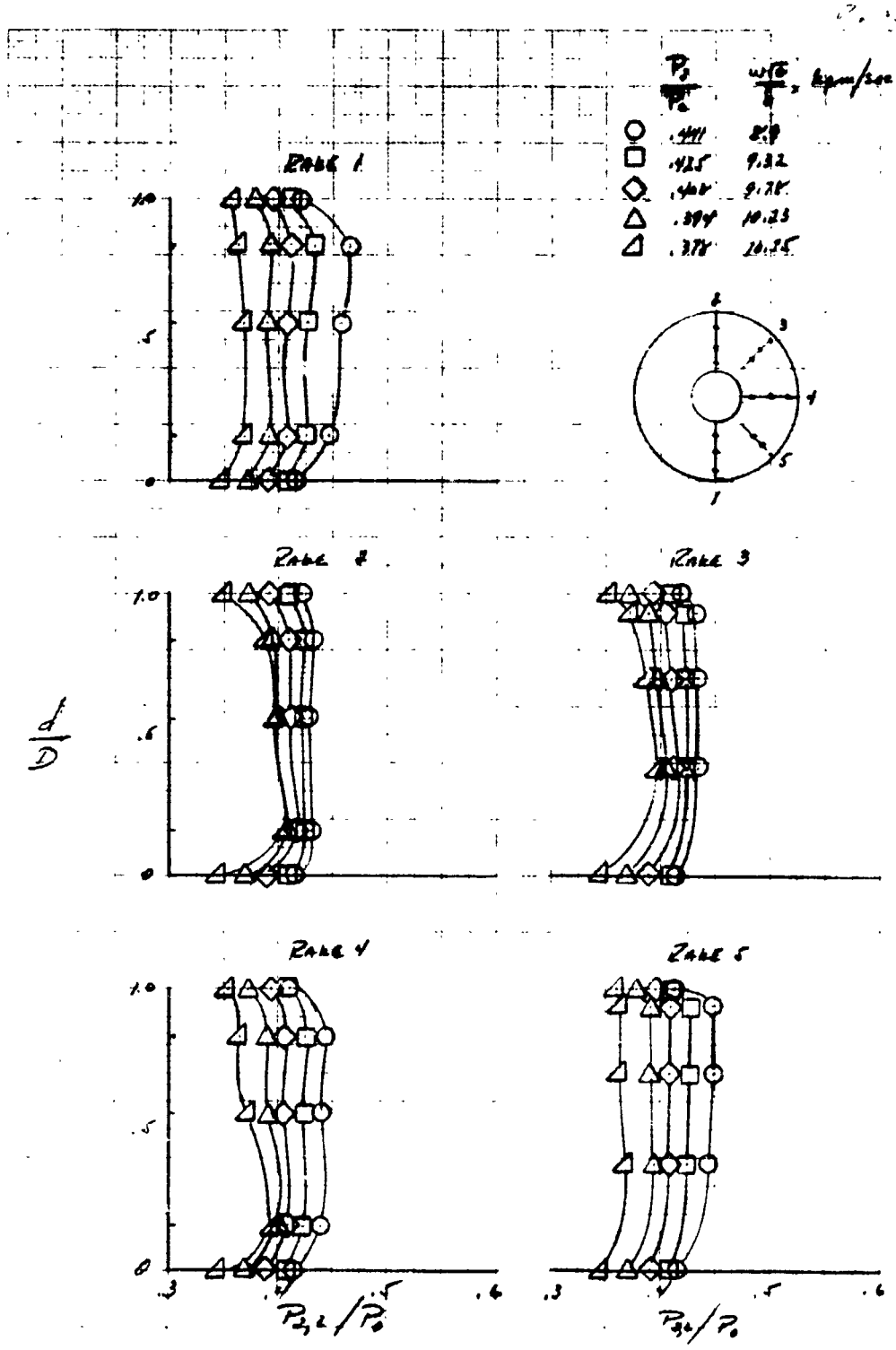

b- $\lambda_1 = 3°$, $\lambda_2 = 18°$, $\lambda_3 = 5°$, $\lambda_4 = -3.1$ cm, $\partial L = 50\%$

FIGURE 16- CONCLUDED.

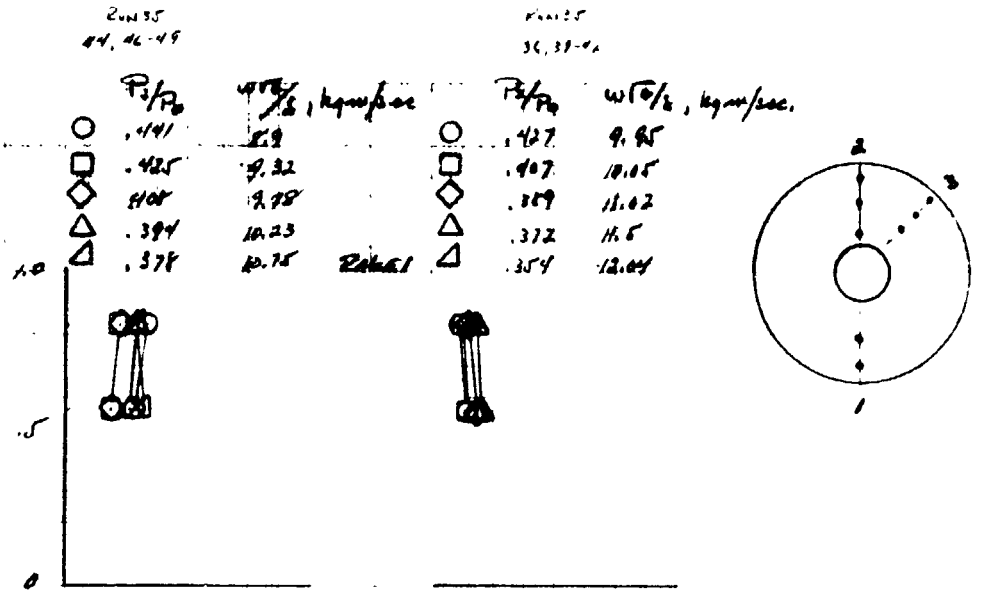

RAKE 2

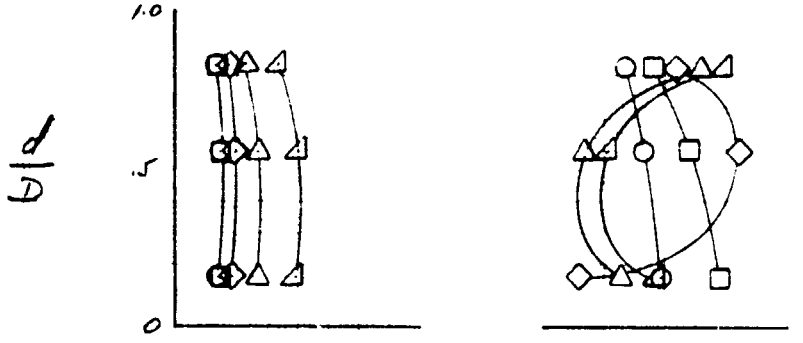

RAKE 3

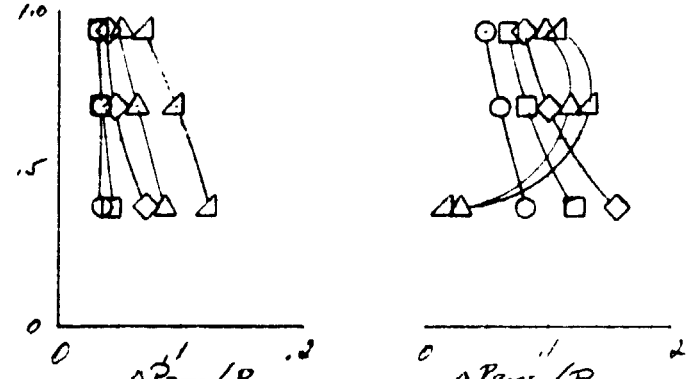

a - $\lambda_1 = 3°$, $\lambda_2 = 14°$, $\lambda_3 = 5°$
$\lambda_4 = -3.1$ cm, BL = 50%

b - $\lambda_1 = 3°$, $\lambda_2 = 15.37°$, $\lambda_3 = 7.5°$
$\lambda_4 = -2.74$ cm, BL = 41%

FIGURE 17. COMPRESSOR FACE DYNAMIC TOTAL PRESSURE PROFILES, $\alpha = 0°$, $\beta = 0°$, $M_0 = 3.52$, $R_L = 7.05 \times 10^6$/m